geosciences

MDPI

Review

A Review of Tsunami Hazards in the Makran Subduction Zone

Amin Rashidi [1,*], Denys Dutykh [2,3], Zaher Hossein Shomali [1,4], Nasser Keshavarz Farajkhah [5] and Mohammadsadegh Nouri [6]

1. Institute of Geophysics, University of Tehran, Tehran 1435944411, Iran; hossein.shomali@geo.uu.se
2. Univ. Grenoble Alpes, Univ. Savoie Mont Blanc, CNRS, LAMA, 73000 Chambéry, France; Denys.Dutykh@univ-smb.fr
3. Mathematics Laboratory (LAMA UMR 5127), Savoie Mont Blanc University, Campus Scientifique, 73376 Le Bourget-du-Lac, France
4. Department of Earth Sciences, Uppsala University, 75236 Uppsala, Sweden
5. Research Institute of Petroleum Industry, Tehran 1485733111, Iran; keshavarzn@ripi.ir
6. School of Civil Engineering, University of Tehran, Tehran 1417613131, Iran; msadegh_nouri@ut.ac.ir

* Correspondence: amin.rashidi@ut.ac.ir

Received: 1 September 2020; Accepted: 16 September 2020; Published: 18 September 2020

Abstract: The uncertain tsunamigenic potential of the Makran Subduction Zone (MSZ) has made it an interesting natural laboratory for tsunami-related studies. This study aims to review the recent activities on tsunami hazard in the Makran subduction zone with a focus on deterministic and probabilistic tsunami hazard assessments. While almost all studies focused on tsunami hazard from the Makran subduction thrust, other local sources such as splay faults and landslides can be also real threats in the future. Far-field tsunami sources such as Sumatra-Andaman and Java subduction zones, commonly lumped as the Sunda subduction zone, do not seem to pose a serious risk to the Makran coastlines. The tsunamigenic potential of the western segment of the MSZ should not be underestimated considering the new evidence from geological studies and lessons from past tsunamis in the world. An overview of the results of tsunami hazard studies shows that the coastal area between Kereti to Ormara along the shoreline of Iran-Pakistan and the coastal segment between Muscat and Sur along Oman's shoreline are the most hazardous areas. Uncertainties in studying tsunami hazard for the Makran region are large. We recommend that future studies mainly focus on the role of thick sediments, a better understanding of the plates interface geometry, the source mechanism and history of extreme-wave deposits, the contribution of other local tsunamigenic sources and vulnerability assessment for all coastlines of the whole Makran region.

Keywords: Makran subduction zone; tsunami hazard; deterministic hazard assessment; probabilistic hazard assessment; uncertainty quantification; numerical modeling

1. Introduction

The Makran Subduction Zone (MSZ) is located where the oceanic crust of the Arabian plate is sliding under the Eurasian plate at a rate of ∼20 mm/year [1]. The future tsunamigenic potential of the Makran subduction zone remains uncertain due to its low and strange offshore seismicity (see Figure 1). In addition, some seismotectonic characteristics of the Makran subduction zone, such as the offshore seismicity, width and dip of the slab, segmentation, partial locking, were frequently debated and questioned. The pattern of offshore seismicity suggests the segmentation of the MSZ into western and eastern parts. There is significant uncertainty about the tsunami hazard along the MSZ with distinct differences in seismicity between the western and eastern segments. According to Mokhtari et al. [2], "This appears to be due to collision of continental crust in the west, in contrast to subduction of oceanic crust in the east". The eastern Makran is a relatively active seismic zone and hosted two instrumentally recorded tsunamis in 1945 (M_w 8.1) and 2013 (M_w 7.7) [3,4]. The western Makran is marked with no major seismicity in recent centuries. According to Rajendran et al. [5]: "The various lines of evidence thus suggest that although the western segment is potentially seismogenic, large earthquakes have not occurred there in the recent past, at least during the last 600 years". It should be noted that the historical records regarding seismicity and tsunamis in the MSZ are very scant. The seismicty of the Makran subduction zone is sparse. The beginning year of complete reporting of earthquakes for Makran was estimated at 1919 in Mirzaei et al. [6]. Rajendran et al. [5] discussed three interpretations for the current seismic status of the western Makran: (1) the whole segment is aseismic, (2) subduction does not occur any more along this segment and (3) the western Makran segment is currently locked and has the potential of producing future great subduction earthquakes. Also, other kinds of evidence such as GPS measurements and the marine terraces gave rise to speculation that there is a possible locked seismogenic zone in the western Makran [3,7].

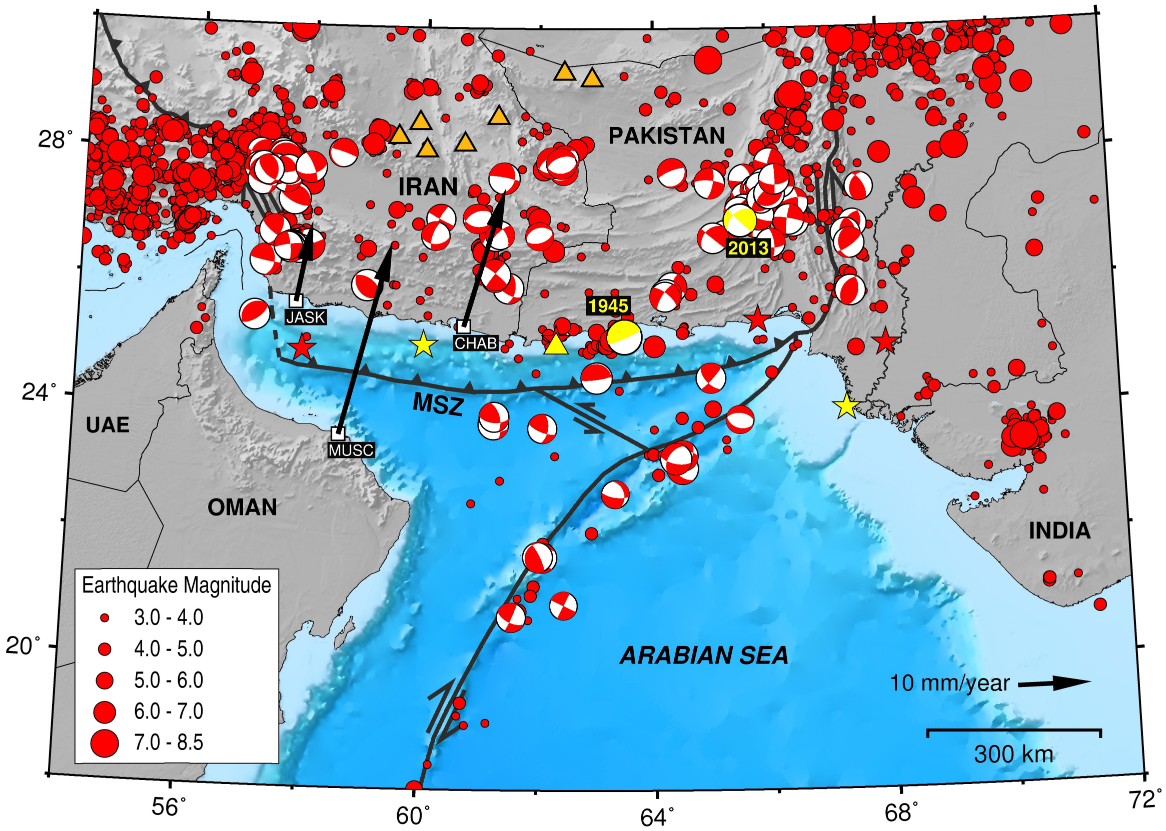

Figure 1. Seismicity of the Makran subduction zone (MSZ). Circles represent earthquakes from 1900 to 2019 from the ISC Catalog. Stars are historical earthquakes (pre-1900) from Heidarzadeh et al. [8]. Orange and yellow triangles represent volcanoes. Tsunamigenic events are illustrated by yellow color. Focal mechanisms are from the Global CMT Catalog. Dashed and solid black lines show the plate boundaries. Black arrows display estimated GPS horizontal velocities for JASK, CHAB, MUSC sites from Vernant et al. [9].

Despite the puzzling tsunamigenic potential, the Makran subduction zone is an excellent natural laboratory for tsunami-related research. This includes a variety of studies such as tsunami history, tsunamigenic sources, tsunami numerical modeling, Tsunami Hazard Assessment (THA) and management, tsunami sedimentology and geomorphology. Increased interest in such studies enhanced our understanding of tsunami hazard in the Makran subduction zone during the last two decades.

This study aims to review the tsunami hazard in the Makran region and to describe the contributions from researchers in assessing tsunami hazard and risk in the MSZ.

This manuscript is organized as follows. Section 2 briefly reviews near-field and far-field tsunami sources that have the potential to generate tsunamis and affect the Makran coastlines. In Section 3, a description of recent work on tsunami hazard assessments in the MSZ is presented. More specifically, Section 3.1 describes the literature on deterministic tsunami hazard assessment and Section 3.2 reviews the recent studies of probabilistic tsunami hazard assessment for the Makran region. Section 4, the discussion, contains addressing uncertainties, limitations and some remarks about the tsunami hazard assessment for the Makran region. Finally, in Section 5, we summarize the key points and offer some practical recommendations for future research directions. These include (1) the contribution of near-field and far-field tsunami sources to the tsunami hazard in Makran; (2) particularly important hazard and uncertainty factors; (3) the importance of detailed risk-based and vulnerability assessments; (4) the necessity of high-resolution topo-bathymetric data.

2. Tsunami Sources in the Makran Subduction Zone

Below we give a brief overview of tsunami sources around the Makran region by dividing them into two main groups: near-field (local and regional) and far-field (distant).

2.1. Near-Field Tsunami Sources in the Makran Subduction Zone

2.1.1. Earthquakes

Earthquakes are the major source for tsunamis in the Makran region similarly to other tsunamigenic zones. The hypocenter location of these earthquakes can be either offshore (e.g., the 1945 tsunami) or onshore (e.g., the 2013 tsunami). However, the fault rupture that generates the tsunami can pass through the coastline. As considered explicitly by Byrne et al. [3], uplift at Ormara implies that the 1945 fault rupture extended beneath the coast. Heidarzadeh et al. [8] presented a catalogue of historical tsunamis in the Makran subduction zone compiling many archival records. Their study is the best reference concerning the history of tsunamis in the MSZ, although there are other studies that mentioned tsunamigenic events in the northwestern Indian Ocean. According to Heidarzadeh et al. [8], Makran experienced at least four tsunamis (in 326 BC, 1008, 1524 and 1897) in addition to the 1945 and 2013 events. Heidarzadeh et al. [8] found that the 1897 event was a volcanic tsunami and the events of 326 BC, 1008 and 1524 were tectonic tsunamis. Alternatively, the 326 BC event resulted from tides, and the 1008 tsunami was sourced in the Persian Gulf [10]. Heidarzadeh et al. [8] concluded that the mean return period for tectonic tsunamis in the MSZ is about 800 years and for a magnitude 8+ earthquake between 100 and 250 years.

The Makran subduction thrust is the main tsunami source in the region. Smith et al. [11] introduced a wide potential seismogenic zone of up to ∼350 km for the MSZ based on thermal modeling. However, they suggested a minimum rupture width of 210 km for the MSZ based on the limit of significant offshore seismicity. The estimated rupture width for the 1945 Makran earthquake is in the range of 70–100 km (e.g., [3,8,12–14]). Frohling and Szeliga [15] proposed a locking depth of 38 km for the MSZ. Consequently, considering an approximate length of 900 km, the MSZ can generate megathrust earthquakes up to M_w 8.8 [15]. According to Nemati [16], the width of the subducting slab is about 120 km in the western and about 150 km in the eastern Makran regions. Nemati [16] suggested a seismogenic depth of ∼90–120 km and ∼160 km for the western and eastern Makran, respectively.

The degree of slip heterogeneity and the location of greatest slip on the rupture area control the power of a tsunamigenic source [17]. Due to the lack of data and the unknown seismic status of the western Makran, there is not a clear idea about how slip may occur during possible future events. However, modeling the recent megathrust events in the world revealed complex and non-uniform ruptures. The MSZ is segmented and the convergence rate changes from west to east along the subduction zone. It is not certain that the strain accumulation along the MSZ is uniform or non-uniform.

The fault-coupling model of Frohling and Szeliga [15] for the MSZ divides it into three segments (i.e., western, central and eastern). The plate coupling ratio in the central part is lower than the western and eastern segments. Ruff and Kanamori [18] suggested that the plate coupling corresponds with the size of asperity [15]. Thus, the fault-coupling model of Frohling and Szeliga [15] may suggest the presence of multiple small asperities along the MSZ. However, Frohling and Szeliga [15] still consider the possibility of a single segment rupture. For example, the Nankai Trough is also segmented, but that did not impede a long rupture in 1707 [19]. Kato [20] remarks that an asperity on a plate boundary is non-uniform and encompassed by aseismic slip. The slip complexity and behavior in a megathrust event are affected by the plate coupling degree, the slab geometry, fluids, slow-slip motions, sediments, the topography of subducting plate and the geology of upper plate [21].

Other important sources for generating local tectonic tsunamis in the Makran regions are splay faults [22]. Although splay faults are small, they are important because they can spread the displacement over a large area and therefore can cause big earthqaukes. Splay faults can break either during the occurrence of megathrust earthquakes or independently of the subduction thrust in which they are rooted [23]. In the well-documented case of the 1964 Alaska earthquake, splay faulting accompanied slip on the master thrust, and the steeper dip of a splay contributed to tsunami generation by producing greater seafloor uplift in its vicinity [24]. Tsunami scenarios can presuppose splay faulting, as a factor of safety, to increase tsunami size (e.g., [25]). Interpretation of seismic profiles revealed a shallow E-W-trending splay fault system along the Makran subduction zone [22,26–28]. The results of numerical modeling show that splay faulting in MSZ can significantly increase the tsunami hazard (e.g., [22,29]). In addition to splay faults, normal faults were also detected in seismic data near the coastline [22,27]. Other candidates for near-field tectonic sources are the Minab-Zendan and Ornach-Nal fault zones, the Murray ridge and the Owen fracture zone (c.f., Figure 2).

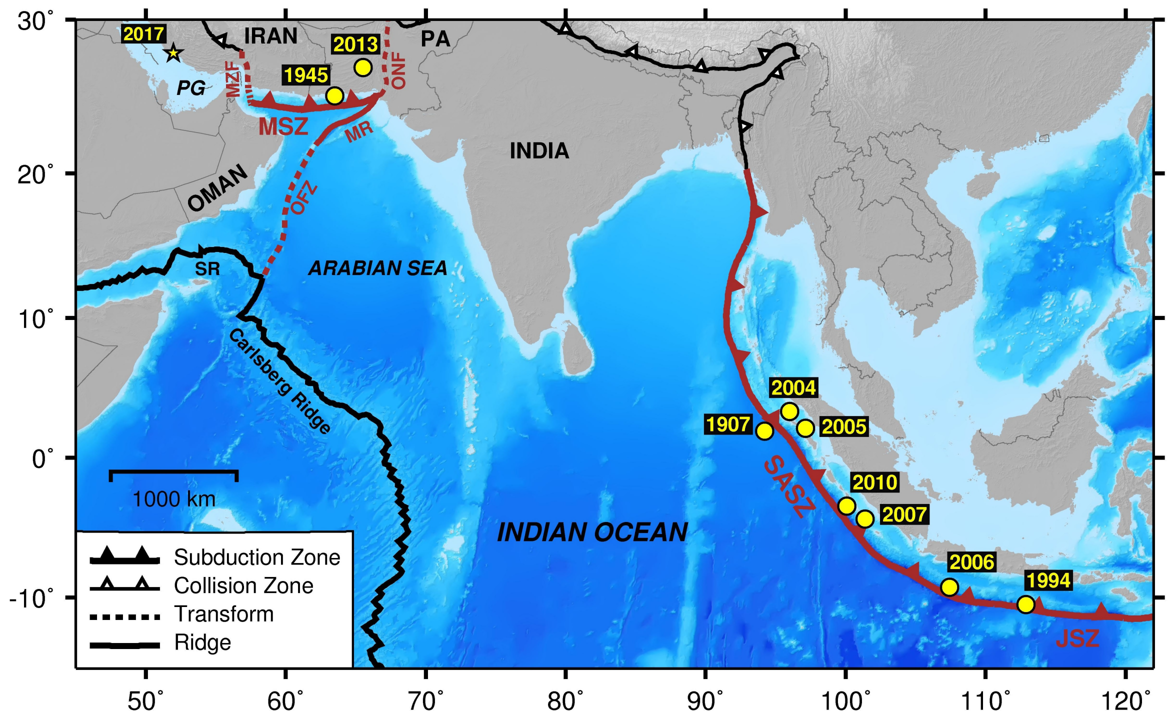

Figure 2. Near-field and Far-field sources around the Makran subduction zone (brown lines) and other plate boundaries (black lines). Yellow circles show the tectonic tsunamis in the Indian Ocean and the yellow star represents the 2017 Persian Gulf meteotsunami. PG Persian Gulf, PA Pakistan, MZF Minab-Zendan Fault, ONF Ornach-Nal Fault, MR Murray Ridge, OFZ Owen Fracture Zone, SR Sheba Ridge, SASZ Sumatra-Andaman Subduction Zone, JSZ Java Subduction Zone.

2.1.2. Landslides

Submarine landslides are the second most important tsunamigenic source. The thick marine sediments can cause submarine failure and make the continental shelf margin in the MSZ potentially susceptible to landslide-generated tsunamis [30]. They may also amplify tsunamis [31]. Furthermore, future earthquakes along the Makran subduction zone can potentially trigger submarine landslides [30]. Submarine landslides can directly generate local tsunamis with high run-ups or be a major contributor to tsunami generation and amplify the wave run-ups of local tsunamis. As shown by data from geological, sedimentological and seismic surveys, Makran is subject to submarine mass movement. It experienced past submarine landslides and slumps in both Iran and Pakistan sides (e.g., [26,32,33]). A primary prevalent way to find areas prone to submarine landslides is the slope gradient map. Submarine mass movements can occur at slopes of 3 to 6 percents or 12 to 30 degrees (see e.g., [34,35]). Based on this criteria, locations of potential areas to produce landslide in the future are shown in Figure 3.

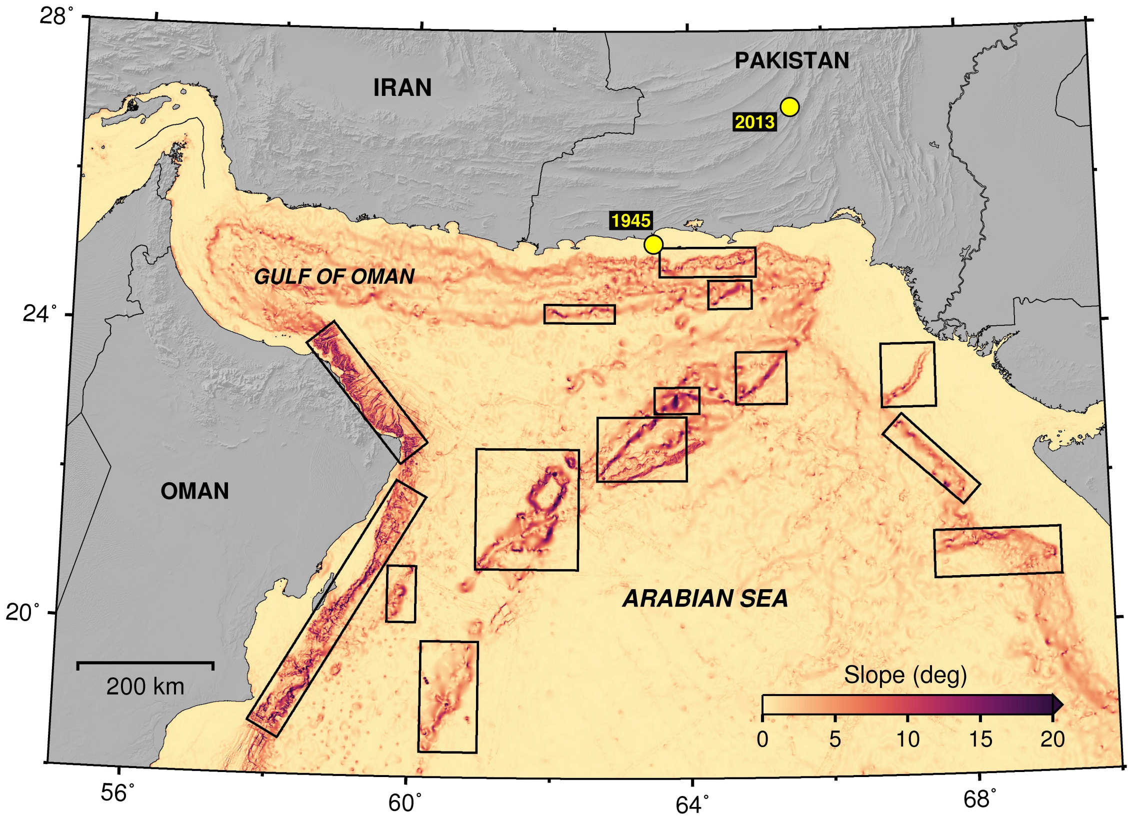

Figure 3. Slope gradient map of the Makran bathymetry and locations of areas prone to submarine landslides (solid black lines). Yellow circles show the locations of the 1945 and 2013 tsunamigenic earthquakes.

Several authors suggested that a triggered submarine landslide by the main shock may be the cause of the delayed arrival and large run-up of the 1945 tsunami waves (e.g., [36–38]). A submarine slump was also a suspect to be responsible for the 2013 Makran tsunami [4]. Deep-water submarine landslides triggered by earthquakes from the active fault system at the Owen fracture zone can potentially generate local tsunamis along the east coast of Oman [39–41].

2.1.3. Volcanic Activities

Volcanic activities can cause tsunamis; however, they are less common. The 1911 Trinidad tsunami is a significant example of a volcano-related tsunami which was caused by explosion of a mud volcano island [4,42]. One of the most iconic features of the MSZ is the presence of many large active mud volcanoes. Snead [43] mentioned that it is possible that the mud volcanoes in the Makan regions are the largest in the world. According to Wiedicke et al. [44], Makran hosted large mud volcanoes with diameters of 1.5–2 km. Four offshore mud volcanoes were formed during the 1945 Makran earthquake [45]. A new island appeared near Gwadar, Pakistan due to the eruption of a mud volcano following the 2013 Makran tsunamigenic earthquake [4]. Heidarzadeh et al. [8] showed that Makran appears to have the potential to generate tsunamis due to submarine volcanoes. They suggested a volcanic origin for the 1897 tsunami in Makran by reviewing historical reports of dead fishes due to some volcanic activities at the time of the event.

2.1.4. Meteorological Tsunamis

Meteorological tsunamis or meteotsunamis are non-seismic tsunami-like waves that are generated by high-energy atmospheric disturbances (e.g., [46,47]). The spatial/temporal characteristics and physical behavior of meteotsunamis and seismic tsunamis are almost the same [48]. The impacts of meteotsunamis are local and they can inundate the coastal areas in the similar way as ordinary tsunamis and can cause human casualties and strong economic losses. A destructive meteotsunami occurred in the Persian Gulf on 19 March 2017 (Figure 2) with a maximum run-up of about 3 m [48]. There is no documented meteotsunami in the Gulf of Oman. Ambraseys and Melville [49] proposed a meteorological origin (ocean storms) for the 1897 Makran tsunami; however, Heidarzadeh et al. [8] doubted this possibility from the evidence of tons of dead fishes. Strong tropical cyclones wereobserved in the Gulf of Oman (e.g., [50,51]). Meteotsunami waves can commonly occur during tropical cyclones [52]. Although no meteotsunami event was identified yet in the Gulf of Oman, distributions of meteotsunamis in the world [47] and new advancements in coastal and marine hazard studies (e.g., [47,48]) indicate the worldwide risk of meteotsunamis.

2.2. Far-Field Tsunami Sources

Far-field tsunami sources that may impact the Makran coastlines are located mostly in far megathrust regions in the Indian Ocean (see Figure 2). The most significant far-field source is the Sumatra–Andaman subduction zone in the Indian Ocean (c.f., Figure 2). The Java subduction zone is the other far-field source in the Indian Ocean (Figure 2). Several destructive tsunamis were generated by these subduction zones (e.g., the 2010 Mentawai, 2006 Java and the 2004 Indian Ocean tsunamis). The results of field surveys and eyewitness reports show that the impacts of the 2004 Indian Ocean tsunami (M_w 9.1) on the Makran coastlines were minor [37,51,53]. Therefore, the far-field sources do not pose a major threat to the Makran coastlines. Other candidates for far-field tectonic sources could be the Sheba and Carlsberg ridges (Figure 2) which were considered in a few tsunami hazard assessment studies so far (e.g., [54,55]).

3. Tsunami Hazard Assessment in the Makran Subduction Zone

Tsunami hazard assessment for coastal areas can be performed using two standard approaches: deterministic and probabilistic. Deterministic Tsunami Hazard Assessment (DTHA) considers a specific scenario (usually the assumed worst-case scenario) and use tsunami numerical modeling to predict the tsunami impact on areas of interest [56]. Probabilistic Tsunami Hazard Assessment (PTHA) considers several potential scenarios and combines the results of tsunami modeling and occurrence rates estimation of tsunamigenic events to determine the hazard level for coastal areas. Tsunami hazard and risk science significantly progressed since the Boxing Day Tsunami in 2004 which led to global growth of scientific research. This includes tsunami numerical modeling of historical tsunamis (e.g., [57,58]) and modern tsunamis such as the 1960 Chile (e.g., [59]), the 1998 Papua New Guinea (e.g., [60]), the 2004 Indian Ocean (e.g., [61,62]), the 2011 Japan (e.g., [63,64]), the 2015 Chile (e.g., [65]) and the 2018 Mexico (e.g., [66]) tsunamis. The other is tsunami numerical modeling and hazard assessment of potential tsunamigenic scenarios in many areas of the world such as the eastern

Japan (e.g., [67]), Chile (e.g., [68]), the western United States (e.g., [69]) and the Mediterranean Sea (e.g., [70]).

Tsunami-related studies for the Makran subduction zone are mostly focused on tsunamigenic potential, historical and modern tsunami history, numerical modeling of occurred and possible tsunamis and tsunami hazard assessment. In the present study, we try to review the recent scientific research with a focus on DTHA and PTHA for the Makran subduction zone. Below, we summarize the recent work on tsunamigenic potential and tsunami history of the MSZ and the DTHA and PTHA studies are separately described in Sections 3.1 and 3.2.

The tsunamigenic potential of the Makran subduction zone has been a subject of interest for seismologists and geologists. Pararas-Carayannis [71] studied the potential of the MSZ for generating tsunamis. The zone has the capability for generating tsunamigenic earthquakes with considerable near and far-field effects [71]. According to Pararas-Carayannis [71], the 1945 Makran tsunamigenic earthquake had a rupture length of about 300–350 km. This is inconsistent with the estimated rupture length of 100–150 km by Byrne et al. [3] and much larger than the lengths reported in other studies such as 200 km in Jaiswal et al. [12], 130 km in Heidarzadeh et al. [72] and 220 km in Heidarzadeh and Satake [14]. Pararas-Carayannis [71] inferred that the magnitude of the 1945 Makran event (M_w 8.1) is the upper limit of earthquakes that the MSZ can generate. The MSZ segmentation and the presence of thick sedimentary layers control the upper limit of earthquakes in this region. The interplate locking within the Makran subduction zone is highly dependent on the degree of consolidation of the sedimentary layers [71]. Some studies analyzed 2D seismic reflection data in Makran to study the relation between the important structural components and the megathrust and tsunamigenic potential of the region (e.g., [2,27]). Mokhtari et al. [2] concluded that the main reason for the lack of trench in the Makran is probably the shallow dip of the subducting plate. The presence of similar marine terraces along eastern and western Makran shorelines may indicate the same tsunamigenic power of both eastern and western Makran [2]. The results of thermal modeling of the Makran region indicate the wide potential seismogenic zone of the MSZ and its ability to produce tsunamigenic earthquakes [11]. According to Smith et al. [11], the thick sediment cover highly increases the temperature between two plates and causes a potential shallow megathrust seismogenic zone. Moreover, Makran is a shallow dip subduction zone which can lead to a wide seismogenic zone capable of generating offshore megathrust earthquakes with magnitudes from M_w 8.7 to 9.2. The study of Smith et al. [11] provides three potential megathrust rupture scenarios in the Makran region which were used in some tsunami hazard assessments (e.g., [17,56]). Analyzing modern and historical seismicity and sedimentary sections has provided important insights into the tsunami potential of the enigmatic western Makran [5]:

- The western Makran has not experienced any major earthquake at least in the last six centuries.
- The recurrence interval of earthquakes in this region might be more than 1000 years.
- The western Makran has the same tectonic potential as the eastern Makran.
- The western Makran is currently locked and perhaps accumulated enough energy to produce a tsunamigenic earthquake.

Evidence of earthquakes and tsunamis can easily hide in coastal geology. For example, deposits of the 2004 tsunami in Thailand provided interesting modern analogs in a post-2004 hunt for deposits of preceding tsunamis. However, nearly all those deposits had been destroyed by burrowing animals (especially crabs). Eventually, after many person weeks of field work, preserved examples were found in a special setting–freshwater, marshy swales [73,74]. In much this way, earthquake and tsunami indicators along the Makran coast were destroyed or thus far overlooked.

Paleotsunami research and coastal geology (e.g., [75–77]) can help to constrain uncertainties in the tsunami history of a region. The analysis of the sedimentary characteristics of deposits in Sur Lagoon, Oman revealed their tsunami origin–the 1945 Makran tsunami [78]. New investigations on coastal boulders along the Iranian coastline of Makran through fieldwork and boulder transport modeling suggest that only a tsunami is capable of transporting the boulders to the land [79]. This may indicate that the western Makran possesses the evidence of paleotsunamis which are probably generated by the MSZ [79]. Similar tsunami-related deposits were found in a field survey along the coastline of the Sultanate of Oman [80]. In both Shah-hosseini et al. [79] and Hoffmann et al. [80], storms are likely underrated as alternatives to tsunamis boulder movers. For instance, cautionary flags in storm-boulder papers introduced by Paris et al. [81], in accounts of boulder transport by tsunami-like bores from 2013 Supertyphoon Haiyan [82–85], in proof that giant boulders were moved by 21st-century storm waves in Ireland [86], and in language for boulder fields on a Caribbean island that faces the Puerto Rico Trench [87]. A comprehensive geological study by Hoffmann et al. [88] consisting of new sedimentological and archaeological evidence suggests that a tsunami impacted the Arabian Sea shorelines about 1000′years ago. They outline a noteworthy conclusion that the possible source for this tsunami could be the western Makran, implying its present-day locking status. The update from Hoffmann et al. [88] adds new evidence from sandy deposits; however the storm alternative is still discounted as inconsistent with storm effects observed only in recent decades.

Over the last decade, admirable efforts were made to understand the effects of the 1945 Makran tsunami through collecting information and interviews with the tsunami survivors. The effects of the 1945 tsunami are summarized by Hoffmann et al. [89] in a review of several types of information including scientific reports, newspaper articles and eyewitness reports to evaluate the impact of the 1945 Makran tsunami on the Makran coastlines. Based on their investigations, they concluded that the death toll of 4000 people [8,90] due to the 1945 Makran tsunami is overestimated and the actual number of deaths is in the order of a couple of hundreds. A field survey was carried out in 2010 to investigate and report the impacts of the 1945 Makran tsunami on the southeastern Iran's coasts [37]. The run-up amplitudes due to the 1945 Makran were estimated at 3 to 7 m (Figure 4) by combining the information from tsunami survivor interviews and field measurements for nine locations along the coastline of Iran [37]. This survey was done more or less in parallel with similar efforts in Oman, Pakistan, and India under the United Nations umbrella. Qualtitative results compiled in an online booklet [91].

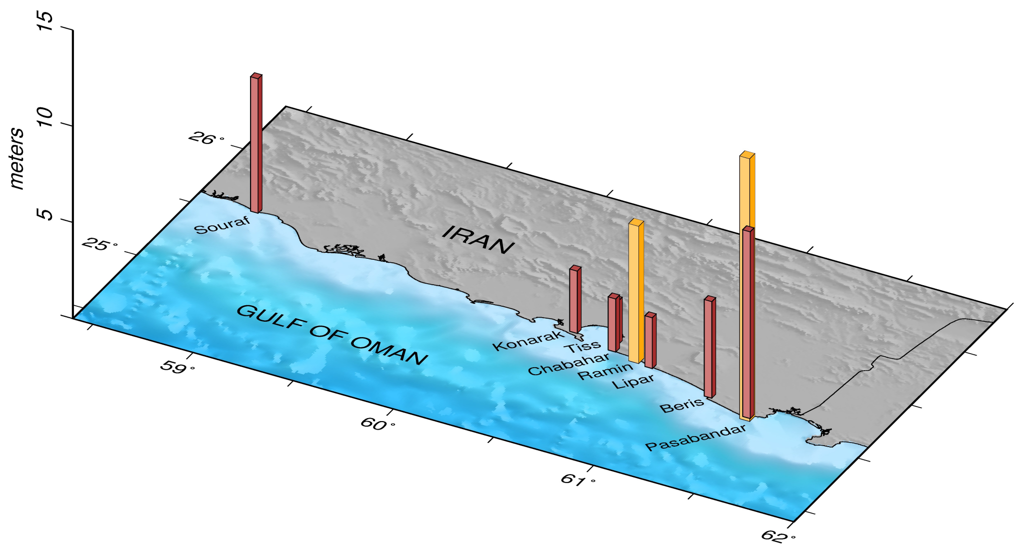

Figure 4. The results of the 2010 fieldwork by Okal et al. [37] in terms of estimated run-up (brown bars) or splash (orange bars) caused by the 1945 Makran tsunami for nine locations along the coastline of Iran (modified after [37]).

The only available instrumental records of the 1945 tsunami are two tide gauge records at Karachi and Mumbai. These two gauges were detided and exploited in numerical modeling studies of the 1945 tsunami [13,14,38]. Recently, Adams et al. [92] detided and analyzed the long version of the Karachi marigram for the 1945 Makran tsunami. They detected an early anomaly before the main shock, through an unconventional detiding manner, and interpreted it as the result of an instrumental or human error, or an earthquake precursor. The tide-gauge maybe also undervalued the maximum tsunami wave height due to a perceived gap in the marigram that likely coincided with the largest wave [92]. As detided in two different ways [13,92], the maximum gauged height is about 0.5 m. The ungauged wave of the marigram gap was probably higher; however, as judged from effects elsewhere in Karachi Harbour [92,93].

3.1. Deterministic Studies

In this section, we review the available literature on deterministic tsunami hazard assessment for the Makran subduction zone. These reviewed works modeled tsunamis for specific scenarios in the Makran region. We classify the DTHA studies into two groups: (1) modeling of real tsunamis in the MSZ and (2) modeling of hypothetical tsunami scenarios in the MSZ.

3.1.1. Modeling of Real Tsunamis in the Makran Subduction Zone

Heidarzadeh et al. [8] simulated the 1945 Makran tsunami and based on the comparison between simulated and observed run-ups concluded that the earthquake cannot be solely responsible for the tsunami. Rajendran et al. [36] used the source parameters provided by Byrne et al. [3] to model the tsunami waves of the 1945 Makran event and compared the simulated arrival times with observed ones. Both studies stated that the contribution of a submarine landslide along with the earthquake to produce large run-up of up to 12–15 m is probable. However, Heidarzadeh et al. [8] proposed two other alternatives including splay faulting and incorrectness of the reports of large run-up heights. Also, they disapproved the idea of a possible larger magnitude for the 1945 Makran tsunami [10] since the reports of the coseismic uplift (∼2 m) are in agreement with the magnitude of M_w 8.1. Arjun et al. [94] simulated the run-up caused by the tsunami of 1945 in order to examine its impact along the southwest coast of India and Lakshadweep islands. Neetu et al. [13] examined the cause of significant waves by this tsunami through numerical modeling and analysis of tide gauge records at Karachi and Mumbai. The trapping of tsunami wave energy on the Makran continental shelf is the cause of the relatively high tsunami waves at Karachi. Neetu et al. [13] concluded that the 1945 earthquake produced the tsunami without contribution of any secondary sources.

Heidarzadeh and Satake [14] employed different methods such as spectral analysis, tsunami forward modeling and tsunami inversion analysis to reach a good fit between simulated and observed waveforms and to achieve an optimized tectonic source model for the 1945 Makran tsunami. They performed a sensitivity analysis to test the effect of source parameters on the tsunami waveforms at Karachi and Mumbai. They found a strike angle of 245° to gain a better match between their computations and the observations. This value is close to the strike angle of 246° from the focal-mechanism solution of Byrne et al. [3], which is oblique to the roughly east-west strike of the plate boundary. Their optimized tectonic source model debatably includes tectonic subsidence at Pasni. Eyewitnesses recalled ejection of reddish water through cracks, along with localized sinking of a harbor area [91]. Phenomena better explained, as in Ambraseys and Melville [49], as effects of seismic shaking, and as tectonic deformation. To reach a better agreement between simulated and observed waveforms, Heidarzadeh and Satake [38] added three different possible secondary sources to the tectonic source of the 1945 tsunami proposed by Heidarzadeh and Satake [14]. These three secondary sources include splay faulting, delayed rupturing and a submarine landslide. They found a combined earthquake-landslide source to give the best match to observations (see Figure 5). The simulated waveforms for the combined source model slightly diverge from the ones for the single tectonic source model. The optimized combined source model reproduced the reported coastal amplitude of ∼12 m [49,95] along a segment of Pakistan's coast [38]. Patel et al. [96] took the source parameters from Byrne et al. [3] to simulate the 1945 tsunami and produce tsunami risk zone maps for the western parts of Gujarat, India. Rastgoftar and Soltanpour [97] examined a submarine landslide as the major source of the 1945 tsunami using numerical modeling and comparison between simulations and reported data. Sarker [98] modeled the 1945 Makran tsunami as an example to discuss impacts of tsunamis on coastal facilities and communities and their associated structural design considerations. Heidarzadeh and Satake [4] performed numerical modeling and analyzed the recorded sea level data to introduce the possible source for the Makran tsunami of 2013. Three different tsunami sources including a mud volcano, diapir and submarine landslide were examined. The results of their numerical modeling suggested a submarine landslide triggered by the inland earthquake was the plausible generator of the 2013 tsunami.

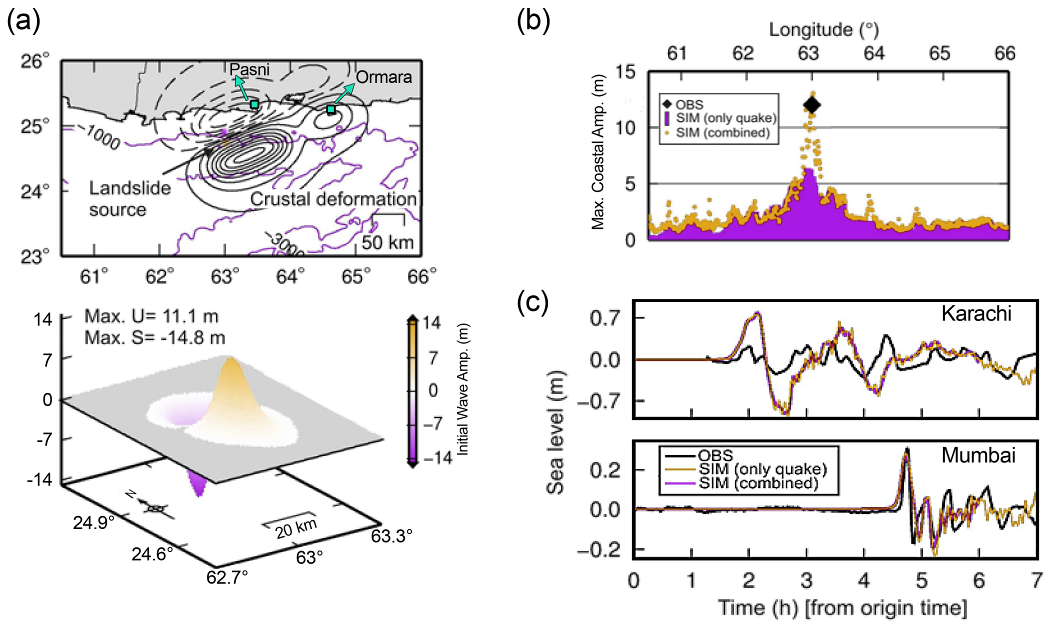

Figure 5. (**a**) The combined earthquake-landslide source proposed by Heidarzadeh and Satake [38] for the 1945 Makran tsunami. Their landslide source has an identical length and width of 15 km and a thickness of 600 m. (**b**) The resultant maximum coastal amplitude from the combined source [38] (**c**) Comparison between the observed and simulated waveforms at Karachi and Mumbai [38]. OBS observed, SIM simulated, U uplift, S subsidence. Modified after Heidarzadeh and Satake [38].

3.1.2. Modeling of Hypothetical Tsunami Scenarios in the Makran Subduction Zone

Okal and Synolakis [99] evaluated far-field tsunami hazard in the Indian Ocean for ten megathrust earthquake scenarios, including two worst-case scenarios of the eastern and the entire MSZ. Heidarzadeh et al. [100] considered six $M8.3$ earthquake scenarios along the Makran subduction zone to perform tsunami numerical modeling in the MSZ. Heidarzadeh et al. [29] conducted inundation modeling for three extreme scenarios in the Makran subduction zone. A preliminary estimation of tsunami hazard was presented by Heidarzadeh et al. [72] for five 1945-type earthquakes (M_w 8.1) scenarios along the MSZ. Based on their results, a 1945-type earthquake may cause coastal amplitudes of 5–7 m along the Iran and Pakistan coastlines.

The effect of Murray ridge (see Figure 2) on tsunami waves from the MSZ was studied by Swapna and Srivastava [41] using numerical modeling. They considered a 1945-type scenario and two scenarios of full lengths of the eastern and western Makran segments. The presence of the Murray ridge changes the directivity, arrival times and amplitudes of tsunami waves towards the south of the MSZ. Payande et al. [101] generated inundation maps for the Chabahar bay, south east of Iran for three tsunami scenarios along the Makran subduction zone. Figure 6a shows a tsunami inundation map of the Chabahar bay for a M_w 9.2 earthquake scenario in the MSZ [101]. All scenarios have an identical epicenter in front of the Chabahar bay in order to radiate the maximum energy of tsunami waves towards Chabahar. They pointed out that the Ω shape of the bay reduces the energy of tsunami waves and the highest waves happen on the exterior coasts of the bay. Browning and Thomas [102] presented a new method for quick initial tsunami hazard assessment in Muscat and Salalah, Oman. Their method includes estimation of run-up and expected maximum loss due to a tsunami using Google Earth and open access GIS and seismic databases. They produced tsunami inundation maps for important coastal segments of Muscat and Salalah (e.g., Figure 6b). Their proposed technique can especially benefit the developing countries and regions with absence of high-resolution bathymetry data. Schneider et al. [103] also developed a modern approach for tsunami flooding risk and vulnerability assessment in Muscat, Oman. They defined a Relative Vulnerability Index (RVI) to grade the vulnerability of buildings to damage by tsunamis.

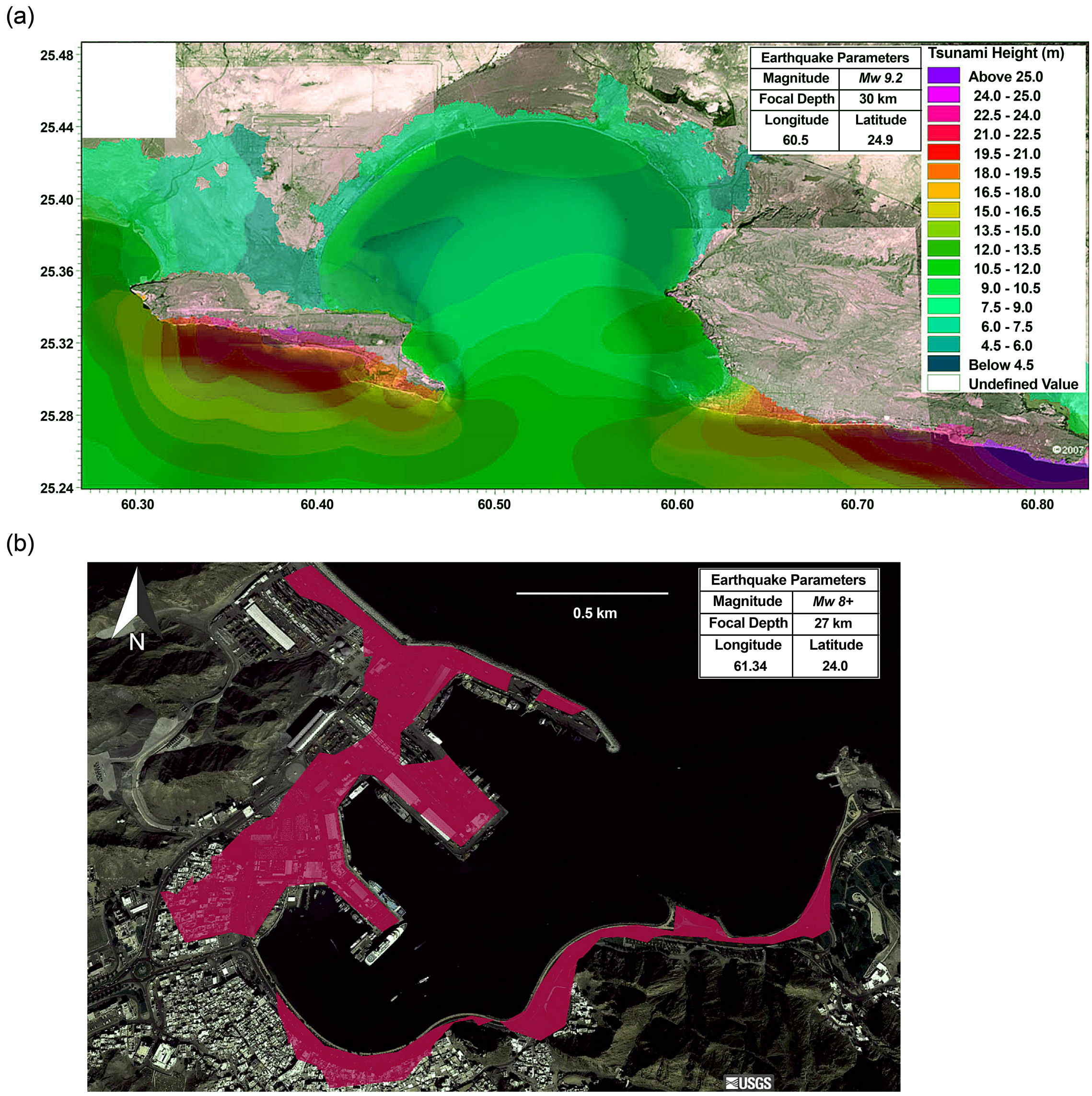

Figure 6. (**a**) Tsunami inundation map for the Chabahar bay, Iran from a M_w 9.2 earthquake scenario in the MSZ (modified after [101]). (**b**) Tsunami inundation map for the Muscat, Oman from a M_w 8+ earthquake scenario in the eastern Makran (modified after [102]).

Suppasri et al. [104] defined four earthquake scenarios in the MSZ and five landslide scenarios inside the Persian Gulf and performed numerical modeling for each scenario to evaluate the deterministic tsunami hazard in the Persian Gulf. Aguirre-Ayerbe et al. [54] developed an integrated tsunami risk assessment approach for the purpose of enhancing the tsunami risk management in Oman considering different site-specific conditions. El-Hussain et al. [105] conducted a deterministic tsunami hazard assessment along the Sur coast of Oman for a worst-case scenario (M_w 8.8) and a 1945-type

(M_w 8.1) earthquakes. Latcharote et al. [106] studied deterministic tsunami hazards in Kuwait and the Persian Gulf for a range of earthquake and landslide tsunami scenarios.

Rashidi et al. [30] estimated the energy of tsunami waves generated by seabed displacement in the near field for a multi-segment source model of the Makran subduction zone. Both static and dynamic generation mechanisms [107] were studied to illustrate the temporal and spatial evolution of tsunami wave energy and exchanges between kinetic and potential energies. A relation between moment magnitude M_w and the total tsunami wave energy was also provided for the entire, western and eastern Makran (see Figure 7). They showed that only a minor portion of the seismic energy can generate a tsunami. Rashidi et al. [108] simulated the propagation and inundation of tsunami waves along the southeastern coastline of Iran for a M_w 8.7 earthquake scenario in the western Makran. Dividing the southeastern Iran into three western, middle and eastern subareas, they showed that the eastern area is more hazardous than the others. To evaluate near-field and far-field tsunami hazards from the western Makran, Rashidi et al. [17] created a source model and developed a novel method to incorporate the slip heterogeneity using scaled slip distributions of some recent tsunamigenic earthquakes (i.e., 2006 Kuril Islands, 2011 Tohoku and 2015 Chile events) into the rupture area. Their results show that a 2011 Tohoku-type event by the western Makran rupture area can cause significant near-field and far-field tsunami hazards (c.f., Figure 8a). Although the western Makran does not seem to have the power to produce such a large earthquake, this hypothesis shows the extreme worst-case scenario from the western Makran. Perhaps, generation of a similar tsunamigenic earthquake to the 2015 Chile event from the western Makran is more plausible (c.f., Figure 8b).

Remark 1. *The middle frame in Figure 8a could be presented to coastal geologists as an outrageous hypothesis for them to test. Coseismic subsidence of 5 m is more than double the subsidence that left lasting intertidal records of giant earthquakes of the 20th century such as 1960 Chile [109] and 1964 Alaska [110]. At Cascadia, micropaleontologists were reckoning coseismic subsidence in 1700 C.E. to be about 1 m or less [111]. These points illustrate a different way that coastal geology might contribute to tsunami hazard assessment at Makran, by providing estimates of coseismic vertical deformation directly relatable to modelers' scenarios for fault rupture and initial condition.*

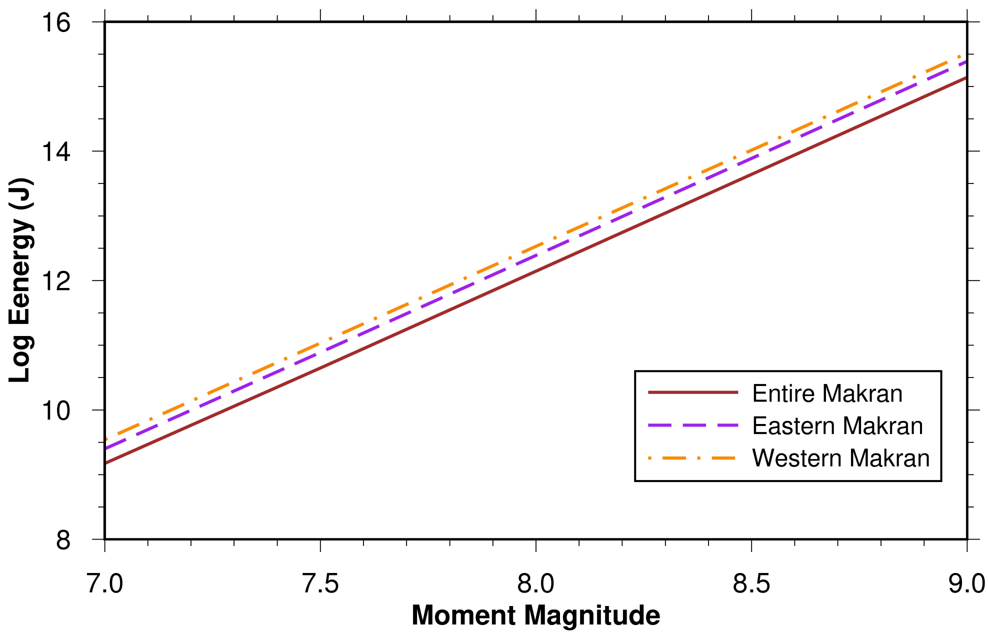

Figure 7. Relationship between moment magnitude and tsunami wave energy for the entire, western and eastern Makran (modified after [30]).

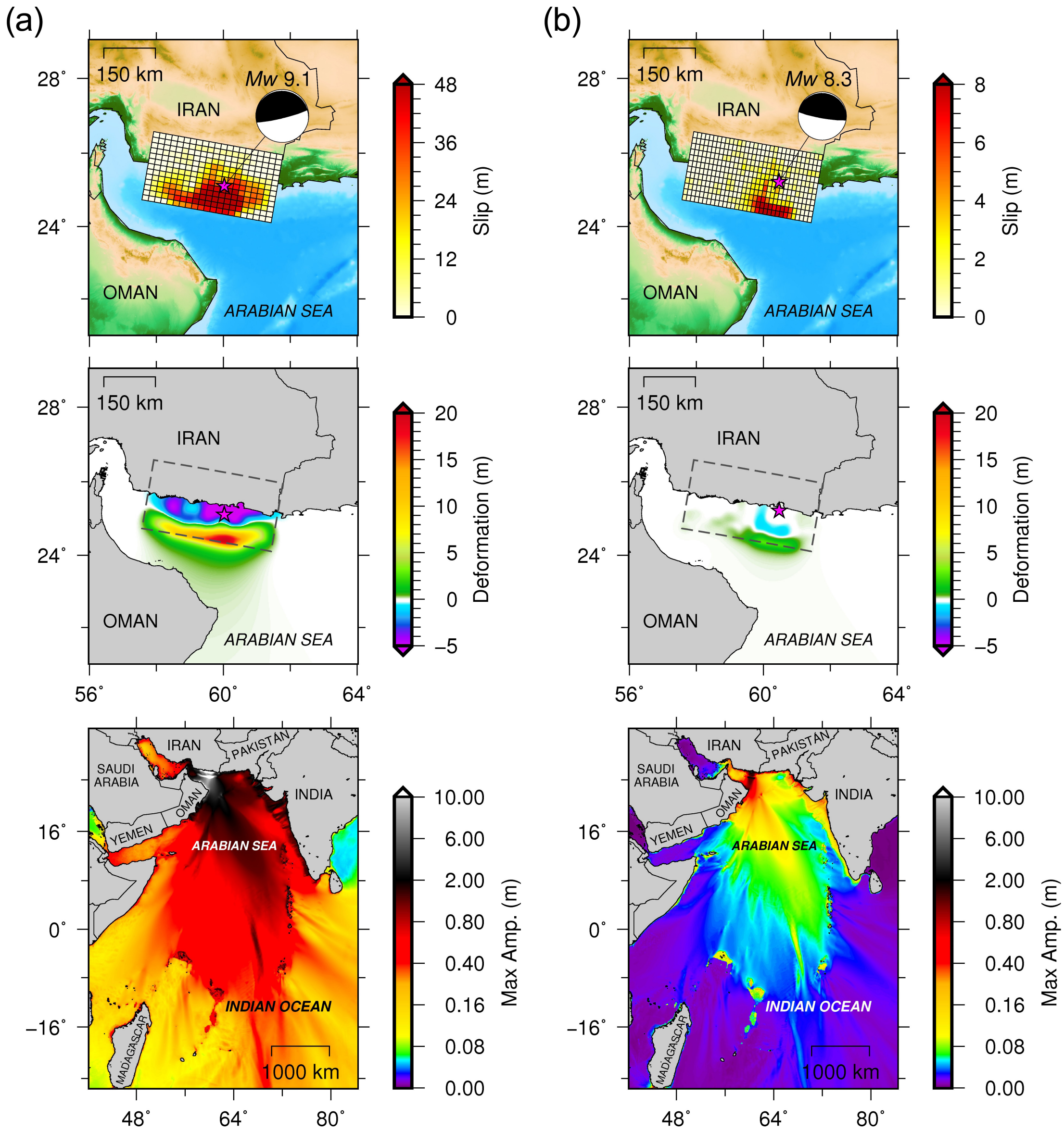

Figure 8. Near-field and far-field tsunami hazard from a 2011 Tohoku-type (**a**) and a 2015 Chile-type (**b**) earthquake scenarios in the western Makran. The top frames show the source models. Purple star is the epicenter. The middle frames show the computed vertical seafloor deformations from the earthquake scenarios. Dashed lines represent the fault plane. The bottom frames show the maximum wave amplitudes from the scenarios. Modified after Rashidi et al. [17].

3.2. Probabilistic Studies

Burbidge et al. [112] presented a PTHA for Indian Ocean nations from three subduction zones of the Makran, Sumatra–Andaman and South Sandwich. For each Indian Ocean nation, they illustrated hazard curves and tsunami hazard maps for a return period of 2000 years. Heidarzadeh and Kijko [113] assessed the tsunami hazard from three 1945-type (M_w 8.1) sources at coastlines of Iran, Pakistan and Oman developing the seismic probabilistic method of Kijko and Sellevoll [114] for tsunamis. They computed tsunami probabilities at some selected sites and along the coastlines of Iran, Pakistan and Oman. They noted that their study is a first generation PTHA for MSZ due to the small number of tsunami sources (three) with equal magnitudes (M_w 8.1). Browning and Thomas [102] introduced a new approach to estimate the probability of the next possible tsunamigenic earthquake in a subduction zone with a similar magnitude.

El-Hussain et al. [115] performed a PTHA for the coast of Oman from a range of small and large scenarios in the MSZ through a logic-tree approach. Their valuable probabilistic study led to a set of probability hazard exceedance maps for the Oman shoreline in different time periods. Hoechner et al. [116] conducted an interesting PTHA for the MSZ and produced probabilistic tsunami hazard curves for the Makran coastlines using different generated synthetic earthquake catalogs for a time length of 300,000 years. They simulated all the events in the catalogs to compute maximum tsunami wave heights along the Makran coastlines and to produce different useful tsunami hazard outcomes including probabilistic tsunami heights and hazard curves (Figure 9a,b). El-Hussain et al. [105] conducted a high resolution PTHA for the coastal segment of Sur, Oman using the earthquake scenario database from El-Hussain et al. [115]. They presented their results in a series of local hazard maps displaying the probability of tsunami wave height/flow depth exceeding different thresholds in given exposure times of 100 and 500 years (see e.g., Figure 10).

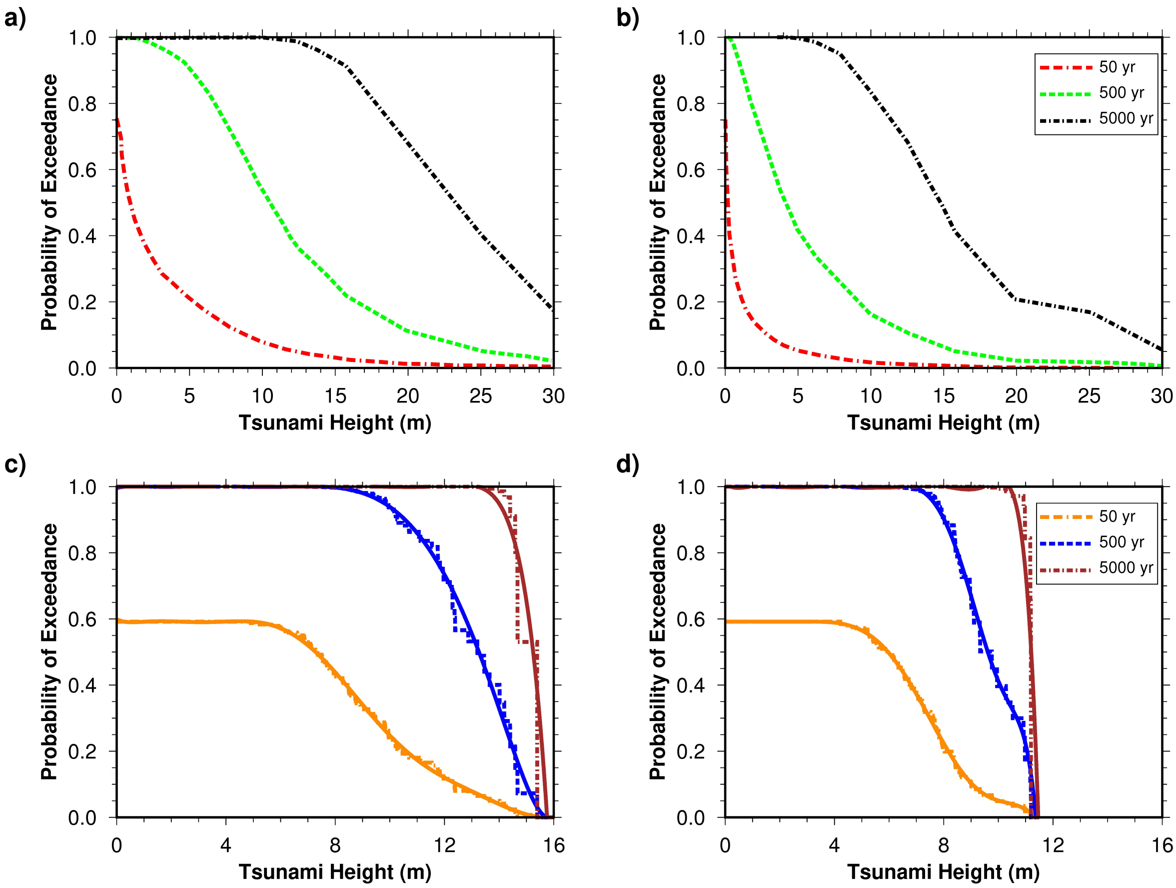

Figure 9. Tsunami hazard curves by Hoechner et al. [116] (**a**,**b**) and Rashidi et al. [56] (**c**,**d**) for coastlines of Iran-Pakistan (left panel) and Oman (right panel).

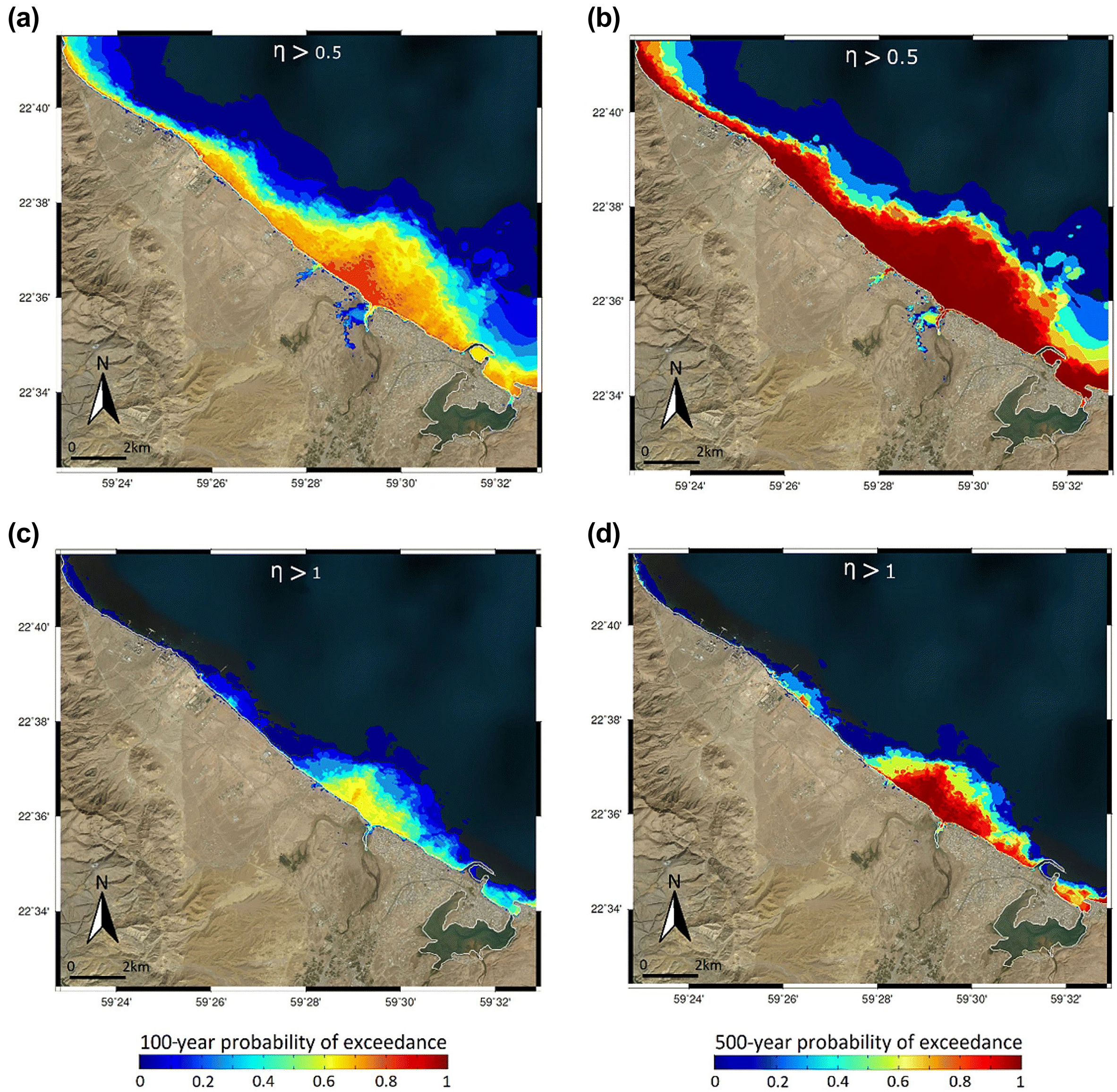

Figure 10. Probability of tsunami wave height/flow depth exceeding 0.5 m (**a**,**b**) and 1 m (**c**,**d**) for time periods of 100 (left panel) and 500 (right panel) years along the coastline of Sur, Oman [105].

Rashidi and Keshavarz Farajkhah [117] employed the probabilistic approach to analyze the tsunami hazard along the southeastern coast of Iran considering a range of magnitudes for the entire, western Makran and eastern Makran tsunamigenic source zones. They generated various tsunami hazard plots such as distributions of probability of exceedance and probabilistic tsunami wave height along the coastline of Iran and hazard curves in different time periods. Rashidi et al. [56] developed an innovative technique through generating a series of random heterogeneous slip models for a non-planar fault geometry of the MSZ and estimated tsunami hazard probabilities along the coastlines of Iran, Pakistan and Oman. They created tsunami probability maps for thresholds of 0.5 and 3 m wave heights over time periods of 50, 250 and 1000 years (see Figure 11) and hazard curves for coastlines of Iran-Pakistan and Oman (see Figure 9c,d). According to Rashidi et al. [56], the slip heterogeneity controls the tsunami wave height and its variation in the near field, especially around the largest asperity on the rupture area.

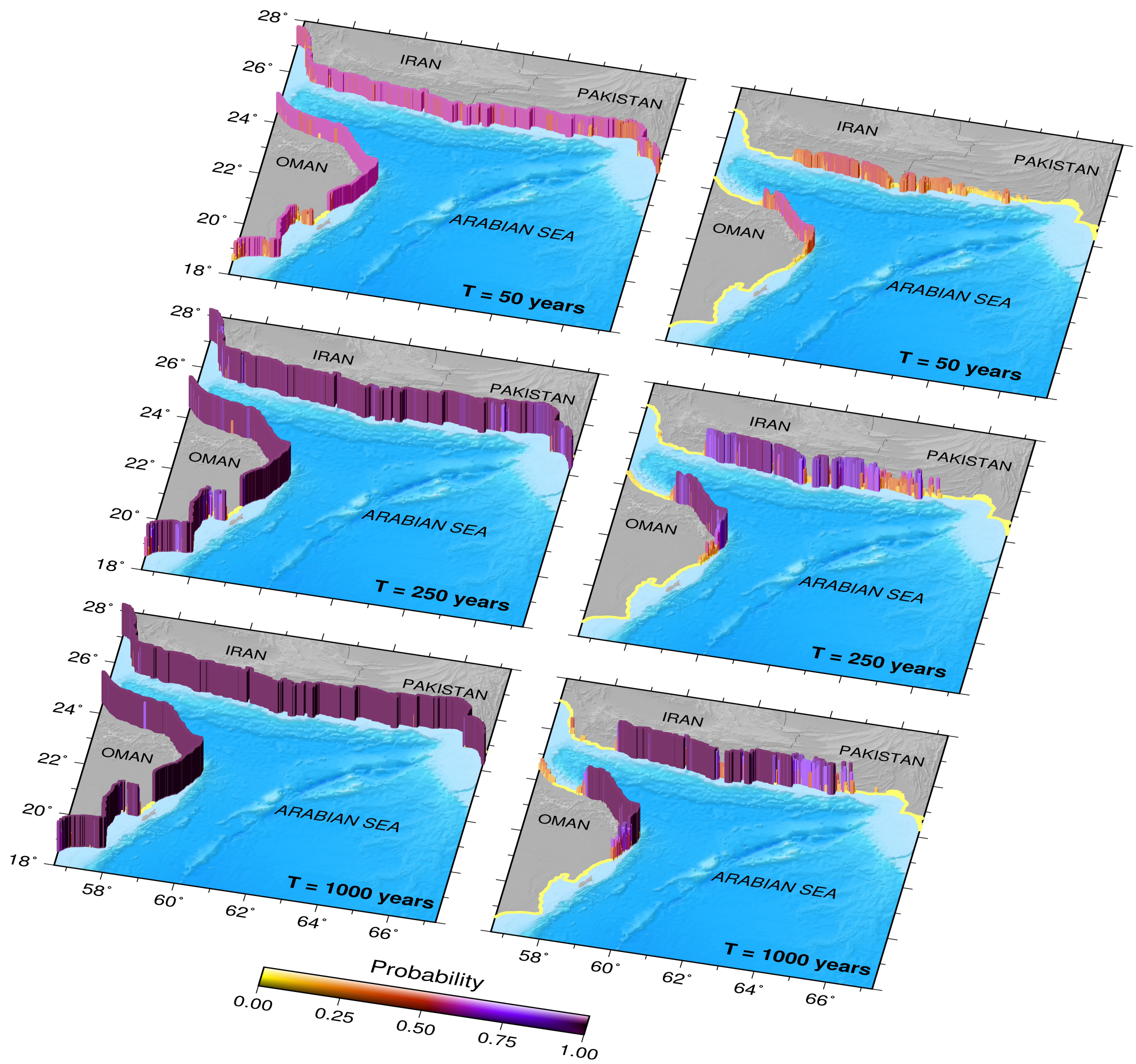

Figure 11. Probability of tsunami wave height exceeding 0.5 m (left panel) and 3 m (right panel) for time periods of 50, 250 and 1000 years along the coastlines of Iran, Pakistan and Oman (modified after [56]).

4. Discussion

As pointed out by Gutscher and Westbrook [118], older models proposed that fast ($\geqslant$4 cm/year) and young (<50 Ma) subduction zones produce larger earthquakes, but the 2004 Indian Ocean tsunami (M_w 9.1) by the Sumatra–Andaman subduction zone (velocity = 2–3 cm/year, age = 60 Ma) was a counterexample. Other researchers also learned that lesson from the 2004 earthquake (e.g., [119,120]) before it was underscored by the 2011 Tohoku event which was an enormous earthquake from subduction of a dinosaur-age (230–65 Myr) part of the Pacific Plate. McCaffrey [120] notes that convergence rate may influence earthquake rate without affecting earthquake size. Makran is a relatively slow (2 cm/year) and old (70 Ma) subduction zone; however, it is theoretically capable of generating great earthquakes [100]. The shallow dip of the MSZ can potentially increase the coupling and provide an appropriate situation for production of large plate boundary events [27,118]. In addition, the thick sedimentation on the incoming plate can also increase the coupling since earthquake asperities can extend to larger depths and pressures [118,121]. Another highlight is regarding the low background seismicity of the MSZ; while there are active subduction zones (e.g., the southwestern Pacific Ocean) with lack of M9 earthquakes since 1900, some subduction zones with low background seismicity (e.g., Nankai, southern Chile) hosted megathrust earthquakes [122].

Several studies indicated the possibility of partial locking of the MSZ (western Makran) and its potential for producing great earthquakes in the future (e.g., [5,11,15,123]).

A key lesson from the 2004 Indian Ocean and 2011 Tohoku tsunamis is that we can never underestimate the behavior and power of a subduction zone. Those events warned us that tsunamigenic events from any vast subduction zone in the world should be anticipated [119,124]. The 2011 Tohoku tsunami showed the errors in the maximum expected earthquake magnitude and the chosen tsunami design height for the tsunami barriers. The 2011 Tohoku tsunami was scarcely anticipated. At least one team of geologists had been studying evidence for its predecessors but the tsunami essentially outraced them [125]. A second such team later emphasized that the enormity of the 2011 tsunami would have been difficult to anticipate from the traces of a predecessor from 869 CE [126]. Before the 2004 Indian Ocean event, it was thought that the Sumatra subduction zone, at least the northern part, would be asleep and no tsunamigenic earthquake would be likely to happen [56]. However, the occurrence of the 2004 catastrophic tsunami violated the previous hypotheses. Recent geological investigations in Thailand, Indonesia, Sri Lanka, India and Tanzania led to discovering tsunami sediment deposits over the last 1000 years (e.g., [127–130]). This shows the importance of sedimentology studies to find past events and investigate the tsunamigenic potential of subduction zones. Extreme-wave deposits were found in recent studies on sediments along the shores of Oman (e.g., [88,131]) suggesting the occurrence of historical tsunamis in the Makran region and especially the potential of the western Makran in producing large ruptures. Such geological studies are also required for shores of Iran and Pakistan. These investigations can also be done by following the examples from other regions in the world. Among examples from other subduction zones, reference could be made to northeasternmost Japan, along the Kuril Trench, where the earthquakes known from historical records (written, instrumental, or both) were associated with moderate tsunamis, in contrast with flooding that ran kilometers inland in the local prehistory of the 17th century CE and earlier [132–134]. Another potential role model is a recent combination of geophysical, documentary, and geological research on a giant 1730 earthquake and tsunami in what is now part of metropolitan Chile [135,136]. The same story as the 2004 and 2011 tsunamis may occur to the MSZ and it would be prudent to plan for or anticipate plausible future events. Ongoing or future risk management may be based on considering the possibility of future plate boundary events by both the western and eastern Makran or even the entire Makran.

4.1. Hazardous Areas

In Tables 1 and 2, we present a general comparison between DTHA and PTHA studies in terms of maximum amplitude and Probability Of Exceedance (POE), respectively. In general, the differences in the results of these studies are mainly due to different source parameters, location, dimension, slip distribution, magnitude-frequency relation, maximum magnitude assumption, number of sources and hydrodynamic model. A review of DTHA and PTHA studies for the MSZ shows that the coastal segment between Muscat and Sur is the hazardous zone along the Oman coastline. To the south of Oman, tsunami waves attenuate, especially due to the presence of the Masirah Island. Several coastal areas along the shores of Iran and Pakistan are more prone to tsunami hazard. These locations are mainly around Kereti, Chabahar, Konarak and Beris along the coastline of Iran and Jiwani, Gwadar, Pasni, Ormara and Karachi at Pakistan.

Table 1. Comparison between computed maximum values of coastal amplitude along the coastlines of Iran (IR), Pakistan (PA) and Oman (OM) from different DTHA studies.

No.	Study	Source Zone	Magnitude (M_w)	Max Amp for IR (m)	Max Amp for PA (m)	Max Amp for OM (m)
1	Heidarzadeh et al. [100]	Makran	8.3	10	∼8	7
2	Heidarzadeh et al. [29]	Eastern Makran Makran	8.6 9.0	3 ∼24	10 ∼20	3 ∼17
3	Heidarzadeh et al. [72]	Makran	8.1	∼7	∼6	∼5
4	El-Hussain et al. [105]	Eastern Makran	8.8	—	8	2
5	Rashidi et al. [108]	Western Makran	8.7	11	—	—
6	Rashidi et al. [17]	Western Makran	8.3 9.0 9.1 8.3	4 41 52 5	2 5 9 2	4 23 38 5
7	Rashidi et al. [56]	Makran	9.1	15	16	12

Table 2. Comparison between estimated maximum values of probability of exceedance (POE) along the coastlines of Iran-Pakistan (IR-PA) and Oman (OM) from different PTHA studies.

No.	Study	Source Zone	Magnitude (M_w) Range	POE (1 m/50 yr) for IR-PA	POE (1 m/50 yr) for OM	POE (1 m/250 yr) for IR-PA	POE (1 m/250 yr) for OM	POE (1 m/500 yr) for IR-PA	POE (1 m/500 yr) for OM	POE (1 m/1000 yr) for IR-PA	POE (1 m/1000 yr) for OM
1	Heidarzadeh and Kijko [113]	Makran	8.1	∼0.45	∼0.45	—	—	—	—	—	—
2	El-Hussain et al. [115]	Makran Western Makran Eastern Makran	7.5–9.1 7.5–8.7 7.5–8.8	—	—	—	0.85	—	∼1	—	1
3	Hoechner et al. [116]	Makran	up to 9.0	∼0.5	∼0.2	—	—	1	∼0.9	—	—
4	Rashidi and Keshavarz Farajkhah [117]	Makran Western Makran Eastern Makran	7.5–9.1 7.5–8.9 7.5–8.9	—	—	—	—	∼1	—	∼1	—
5	Rashidi et al. [56]	Makran	9.06–9.12	0.6	0.6	1	1	—	—	1	1

Based on an overview of tsunami hazard studies for the MSZ, we illustrate an approximate map of tsunami hazard levels along the coastlines of Iran, Pakistan, and Oman (see Figure 12). We note that the presented map only depicts a general outlook of Makran tsunami hazardous areas. The vulnerability of an area to tsunami hazard depends on different factors, including the population density (c.f., Figure 12). Karachi, Chabahar, Muscat and Sohar are ports with the highest population density along the Makran coastlines. The population and economic growth along these coastlines increase their exposure to tsunami risk and imply the importance of vulnerability assessment. Such assessments were conducted for Oman coasts (e.g., [54,103]) for risk management and reduction purposes. As an example, Aguirre-Ayerbe et al. [54] provided useful maps of infrastructure, human and integrated vulnerability levels for Oman (see Figure 13). All Makran nations require official decision maps (e.g., inundation maps, vulnerability assessments, evacuation maps) to be prepared before any possible future disaster.

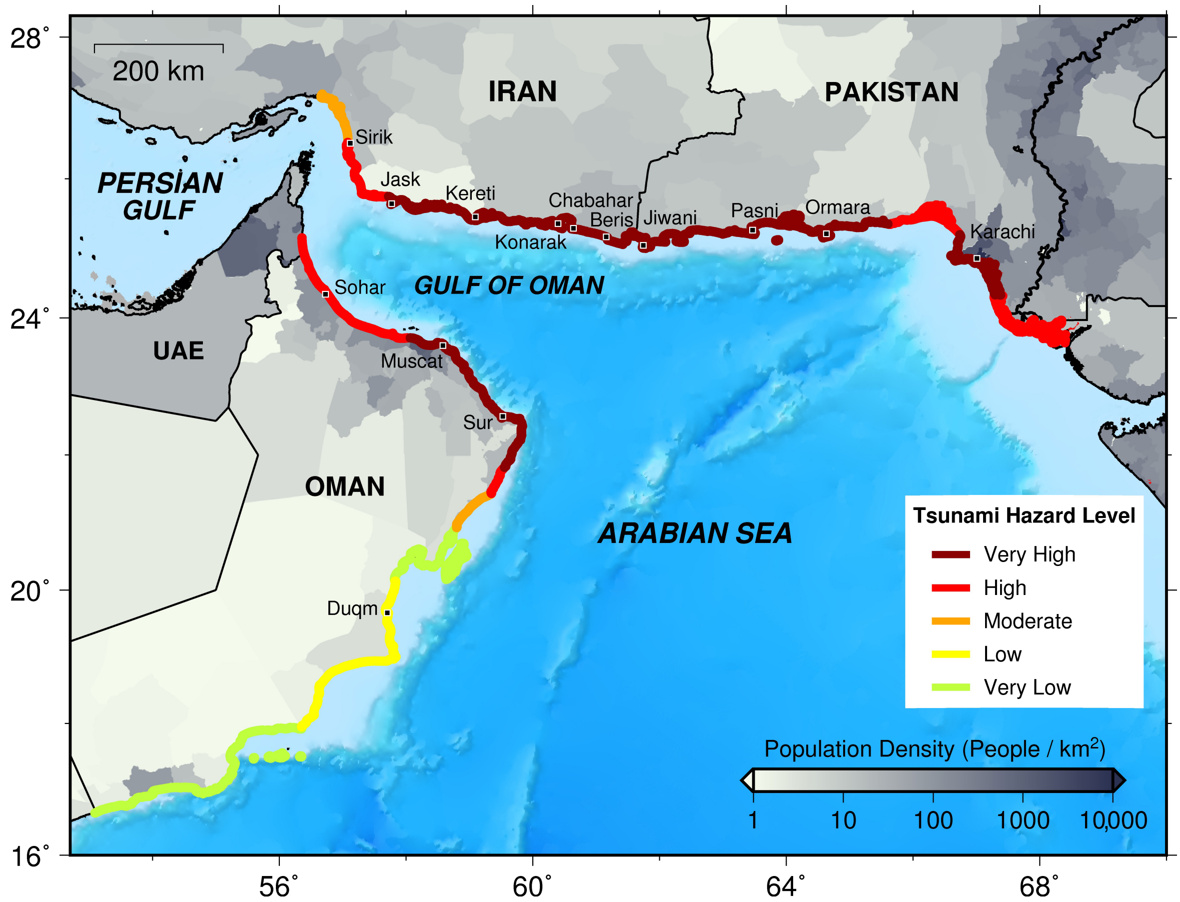

Figure 12. Population denisity [137,138] and tsunami hazard level along the coastlines of the Makran region.

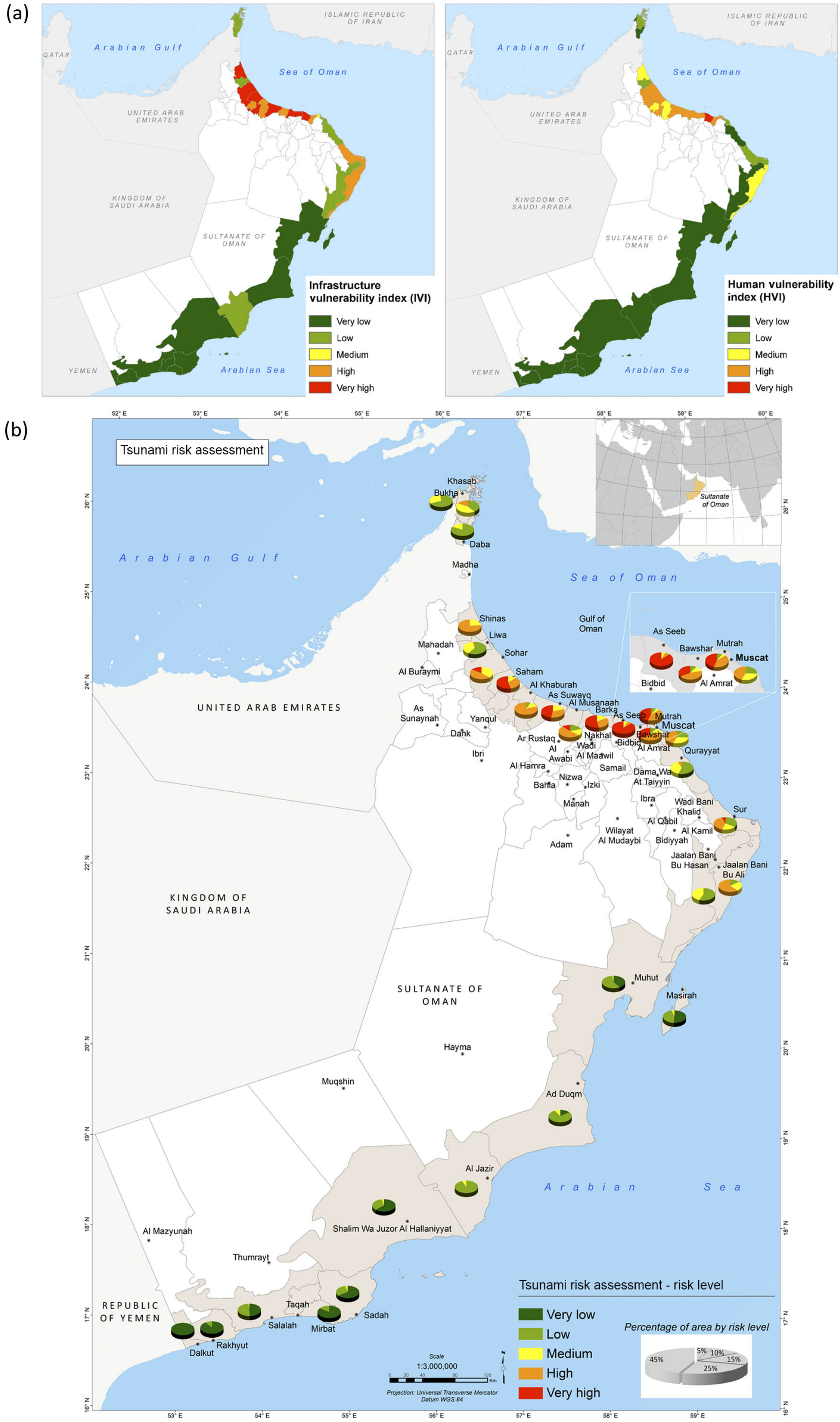

Figure 13. Infrastructure, human (**a**) and integrated (**b**) vulnerability assessments for the Oman coastline [54].

4.2. Uncertainties and Limitations

Uncertainties in a tsunami hazard assessment can be classified into two main groups: aleatory and epistemic uncertainties [139]. Aleatory uncertainties are random and are associated with unpredictability aspects of an event (e.g., source parameters, slip distribution, tides, etc.). Epistemic uncertainties are related to limitations in our knowledge of physical processes [139] in which we can reduce them by enhancing our knowledge, finding new evidence and develop new methods (e.g., rupture segmentation, fault geometry, magnitude-frequency relations, bathymetric data, etc.). In this study, we do not categorize the uncertainties in THA of the MSZ. Here, we only outline the main uncertainties and limitations that might challenge researchers to study the tsunami hazard in the MSZ.

4.2.1. Tsunami Generation

Among different stages of a tsunami, modeling of tsunami generation in the Makran subduction zone possesses the most uncertainties due to the enigmatic tsunamigenic potential of the MSZ. These uncertainties are mostly associated with tsunami scenario definition in the MSZ. Significant part of the MSZ lies beneath the ocean and the lack of hardware technical developments (e.g., marine GPS stations, seafloor sensors, etc.) limits our estimation of the time and location of the next possible subduction zone earthquakes. Moreover, the relative location of the locked sections of the megathrust (especially the western Makran) to the coastal communities is a key factor in the damaging potential of the future events [140]. The absence of adequate geophysical implements does not let us resolve this confusion that whether the western Makran is locked or not.

The potential locking between the down-going and overriding plates can be either partly or entirely and its degree and extent cannot be determined due to the absence of seismicity in the western Makran region [3,88]. The minimum and maximum depths of the slab interface are unknown. The Makran subduction zone appears to have no well-defined trench due to the presence of thick sedimentary layers and also due to the shallow dip (∼2–3°) of the down-going plate [27,141]. Therefore, it was difficult to approximate the geometry of the seismogenic plate interface. Prediction of impacts of future tsunamis depends on the accuracy of the source model especially the geometry of the plate interface. Most studies considered a simple planar geometry for the MSZ or its western and eastern segments. Hoechner et al. [116] and Rashidi et al. [56] are two exceptional studies that assumed a non-planar geometry for the MSZ. Several studies represented a possible plate interface for the MSZ (e.g., [1,3,11,15,142]) that can be used by modelers to setup source model(s) of the MSZ. Recently, Hayes et al. [143] presented 3D geometry models of all active subduction zones in the world, called Slab2, including a slab model of the MSZ. In Figure 14 we plot this model and compare the plate interface from it with three other interfaces from Smith et al. [11], Frohling and Szeliga [15] and Penney et al. [1].

The other uncertainty is regarding the slip distribution of tsunamigenic earthquake sources. Hydrodynamic modeling might not produce the accurate effect of a tsunami if uniform slip is considered for the earthquake source [56]. While the common approach in tsunami modeling is to assume a uniform slip for source models, slip heterogeneity has a key role in distribution and amplitude of tsunami waves in the near field. Only a few studies presented tsunami earthquake scenarios in the MSZ with non-uniform slip distribution (e.g., [14,17,56,116]). Alternative ways to incorporate the rupture complexity in setting up tsunami scenarios could be creating synthetic stochastic slip models and or using slip distributions of other tsunamigenic events in the world. To reduce the uncertainties, more scenario-based studies (e.g., [56,105,115–117]) are essential to consider the most likely sources and to describe the impacts of possible future events in the MSZ.

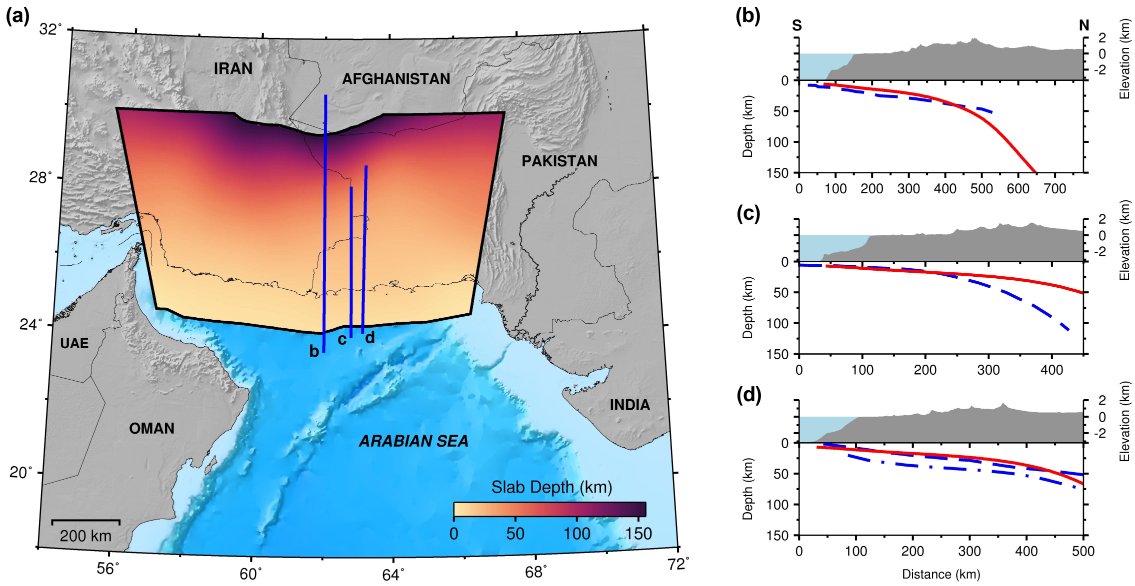

Figure 14. (**a**) Slab2 model for the Makran subduction zone presented by Hayes et al. [143]. Solid blue "a", "b" and "c" lines are profiles from Penney et al. [1], Smith et al. [11] and Frohling and Szeliga [15], respectively, which denote the cross sections of plate interfaces. (**b**) Profile "b" showing cross sections of the plate interface from Penney et al. [1] (dashed blue line) and the Slab2 model (red line). (**c**) Profile "c" showing cross sections of the plate interface from Smith et al. [11] (dashed blue line) and the Slab2 model (red line). (**d**) Profile "d" showing cross sections of the plate interfaces from Frohling and Szeliga [15] (shallow, dashed blue line; deep, dash-dotted blue line) and the Slab2 model (red line).

The above-mentioned issues are major sources of uncertainties that challenge tsunami modelers to define tsunami earthquake scenarios in the Makran region. In addition, the contribution of other tsunamigenic sources such as landslides and splay faults in raising tsunami hazard of the Makran region have not been adequately studied, especially in PTHA. The role of these sources in enhancing tsunami hazard could be either combined with earthquakes from the MSZ or evaluated independently. Recently, Rashidi [22] performed a comprehensive tsunami hazard assessment using both deterministic and probabilistic approaches for the splay faults in the western Makran. According to Grezio et al. [139], there are large uncertainties regarding the probability, possible location and dynamics of landslides basically due to the lack of proper geological data. These uncertainties could be serious challenges for researchers to study and simulate tsunamigenic landslides in the Makran region.

4.2.2. Fault Segmentation

Since the MSZ in seismically segmented into a western and an eastern parts, rupture segmentation has significant implication for the tsunami hazard in the region, especially the maximum magnitude and rupture length [139]. El-Hussain et al. [115] considered two models for rupture in their logic-tree approach, including single rupture by the entire MSZ and segmented ruptures by the western and eastern Makran, and assigned different weights for each model.

4.2.3. Magnitude-Frequency Relation

To perform a PTHA for seismic tsunami sources, annual rates of earthquakes need to be computed usually via the Gutenberg–Richter magnitude-frequency relation: $\log N = a - b \cdot M$ where N is the cumulative number of earthquakes with magnitude $\geqslant M$, a is a constant showing the activity rate and b is the slope of the relation. The magnitude-frequency relation parameters (a and b values) and the assumed maximum magnitude are associated with some uncertainties. Due to the unusual seismicity and uncertain potential of the MSZ, the uncertainty of maximum expected magnitude could be very high for the MSZ. Hoechner et al. [116] showed the dependency of PTHA results on the value of assumed maximum magnitude and variation of the parameters of the Gutenberg–Richter relation. Moreover, another uncertainty for computing magnitude-frequency relation is the seismic zonation [139] as determining the MSZ tectonic boundaries could be challenging due to the uncertainty in its seismicity.

4.2.4. Numerical Modeling

An important challenge that tsunami modelers have to face is the lack of high resolution bathymetry data for the Makran coastlines. Validation of results is another challenge for researchers due to the lack of historical data for the MSZ. There could be also uncertainty over whether the bottom friction should be considered in hydrodynamic modeling or not. Most of experts converge to say that the realistic prediction of tsunami run-up should include bottom friction effects. If the bottom friction is considered, another uncertainty is regarding choosing appropriate value(s) for the Manning's roughness coefficient. However, if we neglect completely the friction effects, the numerical model will slightly overestimate the run-ups, which seems to be a safe and conservative choice for the tsunami hazard assessment. On the other hand, if more accurate estimations are needed, a special hydrodynamic field study is needed to estimate the roughness of the beaches and coasts.

5. Conclusions

Here we present some tentative conclusions and recommendations regarding the tsunami hazard in the Makran subduction zone:

- The near-field tsunami hazard in the northwest Indian Ocean area is mainly controlled by the MSZ; however, the contribution of other near-field sources needs more investigation as they can pose significant future tsunami hazards.
- Far-field tectonic sources may not pose a significant tsunami risk to the Makran coastlines.
- The levels of uncertainties for performing tsunami hazard studies in the MSZ are high due to the lack of detailed data and knowledge especially on the geometry of the plate interface.
- Paleotsunami research, coastal geology and analysis of extreme-wave deposits have also very important implications for tsunami hazard assessment. They can reduce or remove uncertainties about age, location, mechanism and potential of the source of deposits.
- Although significant progress for understanding the tsunami hazard of the MSZ was achieved recently, more scenario-based studies are required to lower the uncertainties and anticipate possible impacts of future events.
- Most tsunami hazard studies in the MSZ are deterministic and thus, more detailed probabilistic risk-based assessments are required to achieve better perspectives of future events.
- To implement the results of deterministic and probabilistic tsunami hazard assessments in the Makran region, more and better data are required. Numerous numerical studies for this region suffer from the lack of high-resolution site-specific topo-bathymetric data.

Perspectives

Future research directions may be focused on:

- Characteristics of thick sediments of the MSZ as they can have undeniable implications on the future tsunami hazard in the MSZ.
- Achieving a better image of the subduction geometry.
- Conducting more studies on extreme-wave deposits and paleotsunami research along the coastlines of Makran.
- Detailed vulnerability assessments for all coastlines of Makran taking into account different human and economic factors.
- Hazard potential of other tsunamigenic sources such as splay faults, submarine landslides and meteotsunamis in this region. Meteotsunamis can be a subject of future research as they are

an underrated hazard that may pose hazard to the coastlines of the Persian Gulf and the Gulf of Oman.

Author Contributions: Conceptualization, Project administration, Validation: A.R. and D.D.; Writing—review & editing: A.R., D.D. and Z.H.S.; Investigation, Writing—original draft: A.R.; Supervision: Z.H.S. and N.K.F.; Visualization: A.R. and M.N. All authors have read and agreed to the published version of the manuscript.

Funding: D.D.'s work has been supported by the French National Research Agency, through Investments for Future Program (ref. ANR-18-EURE-0016-528 Solar Academy).

Acknowledgments: We would like to express our gratitude to the authors of all cited publications in this research for all their valuable efforts and prestigious studies. The Authors express their gratitude to the editor, Richard Li and to both Referees for helping us to improve the manuscript quality and completeness. A.R. and D.D. thank Lauren F. Gowdie for her help and support. Some figures were created using the GMT software [144]. The Gridded Population of the World, Version 4 (GPWv4): Population Density, Revision 11 data were developed by the Center for International Earth Science Information Network (CIESIN), Columbia University and were obtained from the NASA Socioeconomic Data and Applications Center (SEDAC).

Conflicts of Interest: The authors declare no conflict of interest.

Abbreviations

The following abbreviations are used in this manuscript:

MSZ	Makran Subduction Zone
GPS	Global Positioning System
ISC	International Seismological Centre
CMT	Centroid-Moment-Tensor
THA	Tsunami Hazard Assessment
DTHA	Deterministic Tsunami Hazard Assessment
PTHA	Probabilistic Tsunami Hazard Assessment
GIS	Geographic Information System
RVI	Relative Vulnerability Index
M	Magnitude
POE	Probability Of Exceedance
IR	Iran
PA	Pakistan
OM	Oman
PG	Persian Gulf
MZF	Minab-Zendan Fault
ONF	Ornach-Nal Fault
MR	Murray Ridge
OFZ	Owen Fracture Zone
SR	Sheba Ridge
SASZ	Sumatra-Andaman Subduction Zone
JSZ	Java Subduction Zone
ANR	Agence Nationale de la Recherche
GMT	Generic Mapping Tools
GPWv4	Gridded Population of the World, Version 4
CIESIN	Center for International Earth Science Information Network
SEDAC	Socioeconomic Data and Applications Center

References

1. Penney, C.; Tavakoli, F.; Saadat, A.; Nankali, H.R.; Sedighi, M.; Khorrami, F.; Sobouti, F.; Rafi, Z.; Copley, A.; Jackson, J.; et al. Megathrust and accretionary wedge properties and behaviour in the Makran subduction zone. *Geophys. J. Int.* **2017**, *209*, 1800–1830. [CrossRef]
2. Mokhtari, M.; Abdollahie Fard, I.; Hessami, K. Structural elements of the Makran region, Oman sea and their potential relevance to tsunamigenisis. *Nat. Hazards* **2008**, *47*, 185–199. [CrossRef]

3. Byrne, D.E.; Sykes, L.R.; Davis, D.M. Great thrust earthquakes and aseismic slip along the plate boundary of the Makran Subduction Zone. *J. Geophys. Res.* **1992**, *97*, 449–478. [CrossRef]
4. Heidarzadeh, M.; Satake, K. Possible sources of the tsunami observed in the northwestern Indian Ocean following the 2013 September 24 Mw 7.7 Pakistan inland earthquake. *Geophys. J. Int.* **2014**, *199*, 752–766. [CrossRef]
5. Rajendran, C.P.; Rajendran, K.; Shah-hosseini, M.; Beni, A.N.; Nautiyal, C.M.; Andrews, R. The hazard potential of the western segment of the Makran subduction zone, northern Arabian Sea. *Nat. Hazards* **2013**, *65*, 219–239. [CrossRef]
6. Mirzaei, N.; Gao, M.T.; Chen, Y.T.; Wang, J. A uniform catalog of earthquakes for seismic hazard assessment in Iran. *Acta Seismol. Sin.* **1997**, *10*, 713–726. [CrossRef]
7. Masson, F.; Anvari, M.; Djamour, Y.; Walpersdorf, A.; Tavakoli, F.; Daignières, M.; Nankali, H.; Van Gorp, S. Large-scale velocity field and strain tensor in Iran inferred from GPS measurements: New insight for the present-day deformation pattern within NE Iran. *Geophys. J. Int.* **2007**, *170*, 436–440. [CrossRef]
8. Heidarzadeh, M.; Pirooz, M.D.; Zaker, N.H.; Yalciner, A.C.; Mokhtari, M.; Esmaeily, A. Historical tsunami in the Makran Subduction Zone off the southern coasts of Iran and Pakistan and results of numerical modeling. *Ocean Eng.* **2008**, *35*, 774–786. [CrossRef]
9. Vernant, P.; Nilforoushan, F.; Hatzfeld, D.; Abbassi, M.R.; Vigny, C.; Masson, F.; Nankali, H.; Martinod, J.; Ashtiani, A.; Bayer, R.; et al. Present-day crustal deformation and plate kinematics in the Middle East constrained by GPS measurements in Iran and northern Oman. *Geophys. J. Int.* **2004**, *157*, 381–398. [CrossRef]
10. Dominey-Howes, D.; Cummins, P.; Burbidge, D. Historic records of teletsunami in the Indian Ocean and insights from numerical modelling. *Nat. Hazards* **2007**, *42*, 1–17. [CrossRef]
11. Smith, G.L.; McNeill, L.C.; Wang, K.; He, J.; Henstock, T.J. Thermal structure and megathrust seismogenic potential of the Makran subduction zone. *Geophys. Res. Lett.* **2013**, *40*, 1528–1533. [CrossRef]
12. Jaiswal, R.K.; Singh, A.P.; Rastogi, B.K. Simulation of the Arabian Sea Tsunami propagation generated due to 1945 Makran Earthquake and its effect on western parts of Gujarat (India). *Nat. Hazards* **2009**, *48*, 245–258. [CrossRef]
13. Neetu, S.; Suresh, I.; Shankar, R.; Nagarajan, B.; Sharma, R.; Shenoi, S.S.; Unnikrishnan, A.S.; Sundar, D. Trapped waves of the 27 November 1945 Makran tsunami: Observations and numerical modeling. *Nat. Hazards* **2011**, *59*, 1609–1618. [CrossRef]
14. Heidarzadeh, M.; Satake, K. New Insights into the Source of the Makran Tsunami of 27 November 1945 from Tsunami Waveforms and Coastal Deformation Data. *Pure Appl. Geophys.* **2015**, *172*, 621–640. [CrossRef]
15. Frohling, E.; Szeliga, W. GPS constraints on interplate locking within the Makran subduction zone. *Geophys. J. Int.* **2016**, *205*, 67–76. [CrossRef]
16. Nemati, M. Seismotectonic and seismicity of Makran, a bimodal subduction zone, SE Iran. *J. Asian Earth Sci.* **2019**, *169*, 139 – 161. [CrossRef]
17. Rashidi, A.; Shomali, Z.H.; Keshavarz Farajkhah, N. Tsunami Simulations in the Western Makran Using Hypothetical Heterogeneous Source Models from World's Great Earthquakes. *Pure Appl. Geophys.* **2018**, *175*, 1325–1340. [CrossRef]
18. Ruff, L.; Kanamori, H. Seismic coupling and uncoupling at subduction zones. *Tectonophysics* **1983**, *99*, 99–117. [CrossRef]
19. Garrett, E.; Fujiwara, O.; Garrett, P.; Heyvaert, V.M.; Shishikura, M.; Yokoyama, Y.; Hubert-Ferrari, A.; Brückner, H.; Nakamura, A.; De Batist, M. A systematic review of geological evidence for Holocene earthquakes and tsunamis along the Nankai-Suruga Trough, Japan. *Earth-Sci. Rev.* **2016**, *159*, 337–357. [CrossRef]
20. Kato, N. A possible explanation for difference in stress drop between intraplate and interplate earthquakes. *Geophys. Res. Lett.* **2009**, *36*, L23311. [CrossRef]
21. Bilek, S.L.; Lay, T. Subduction zone megathrust earthquakes. *Geosphere* **2018**, *14*, 1468–1500. [CrossRef]
22. Rashidi, A. Numerical Simulation and Hazard Assessment of the Effect of Tsunamigenic Scenarios on the Western Makran Region Using Structural Detection and Restoration. Ph.D. Thesis, University of Tehran, Tehran, Iran, 2018.
23. Li, S.; Moreno, M.; Rosenau, M.; Melnick, D.; Oncken, O. Splay fault triggering by great subduction earthquakes inferred from finite element models. *Geophys. Res. Lett.* **2014**, *41*, 385–391. [CrossRef]

24. Plafker, G. *Tectonics of the March 27, 1964, Alaska Earthquake: Chapter I in the Alaska Earthquake, March 27, 1964: Regional Effects*; US Government Printing Office: Washington, DC, USA, 1969. [CrossRef]
25. Witter, R.C.; Zhang, Y.J.; Wang, K.; Priest, G.R.; Goldfinger, C.; Stimely, L.; English, J.T.; Ferro, P.A. Simulated tsunami inundation for a range of Cascadia megathrust earthquake scenarios at Bandon, Oregon, USA. *Geosphere* **2013**, *9*, 1783–1803. [CrossRef]
26. Grando, G.; McClay, K. Morphotectonics domains and structural styles in the Makran accretionary prism, offshore Iran. *Sediment. Geol.* **2007**, *196*, 157–179. [CrossRef]
27. Smith, G.; McNeill, L.; Henstock, I.J.; Bull, J. The structure and fault activity of the Makran accretionary prism. *J. Geophys. Res. Solid Earth* **2012**, *117*. [CrossRef]
28. Mokhtari, M. The role of splay faulting in increasing the devastation effect of tsunami hazard in Makran, Oman Sea. *Arab. J. Geosci.* **2015**, *8*, 4291–4298. [CrossRef]
29. Heidarzadeh, M.; Pirooz, M.D.; Zaker, N.H. Modeling the near-field effects of the worst-case tsunami in the Makran subduction zone. *Ocean Eng.* **2009**, *36*, 368–376. [CrossRef]
30. Rashidi, A.; Shomali, Z.H.; Dutykh, D.; Keshavarz Faraj Khah, N. Evaluation of tsunami wave energy generated by earthquakes in the Makran subduction zone. *Ocean Eng.* **2018**, *165*, 131–139. [CrossRef]
31. Dutykh, D.; Dias, F. Influence of sedimentary layering on tsunami generation. *Comput. Methods Appl. Mech. Eng.* **2010**, *199*, 1268–1275. [CrossRef]
32. Kukowski, N.; Schillhorn, T.; Huhn, K.; von Rad, U.; Husen, S.; Flueh, E.R. Morphotectonics and mechanics of the central Makran accretionary wedge off Pakistan. *Mar. Geol.* **2001**, *173*, 1–19. [CrossRef]
33. Bourget, J.; Zaragosi, S.; Ellouz-Zimmermann, S.; Ducassou, E.; Prins, M.; Garlan, T.; Lanfumey, V.; Schneider, J.L.; Rouillard, P.; Giraudeau, J. Highstand vs. lowstand turbidite system growth in the Makran active margin: Imprints of high-frequency external controls on sediment delivery mechanisms to deep water systems. *Mar. Geol.* **2010**, *274*, 187–208. [CrossRef]
34. Skempton, A.W. Soil Mechanics relation to geology. *Proc. Yorks. Geol. Soc.* **1953**, *29*, 33–62. [CrossRef]
35. Salaree, A.; Okal, E.A. Field survey and modelling of the Caspian Sea tsunami of 1990 June 20. *Geophys. J. Int.* **2015**, *201*, 621–639. [CrossRef]
36. Rajendran, C.P.; Ramanamurthy, M.V.; Reddy, N.T.; Rajendran, K. Hazard implications of the late arrival of the 1945 Makran tsunami. *Curr. Sci.* **2008**, *95*, 1739–1743.
37. Okal, E.A.; Fritz, H.M.; Hamzeh, M.A.; Ghasemzadeh, J. Field Survey of the 1945 Makran and 2004 Indian Ocean Tsunamis in Baluchistan, Iran. *Pure Appl. Geophys.* **2015**, *172*, 3343–3356. [CrossRef]
38. Heidarzadeh, M.; Satake, K. A Combined Earthquake–Landslide Source Model for the Tsunami from the 27 November 1945 Mw 8.1 Makran Earthquake. *Bull. Seismol. Soc. Am.* **2017**, *107*, 1033–1040. [CrossRef]
39. Fournier, M.; Chamot-Rooke, N.; Rodriguez, M.; Huchon, P.; Petit, C.; Beslier, M.; Zaragosi, S. Owen Fracture Zone: The Arabia–India plate boundary unveiled. *Earth Planet. Sci. Lett.* **2011**, *302*, 247 –252. [CrossRef]
40. Rodriguez, M.; Chamot-Rooke, N.; Hébert, H.; Fournier, M.; Huchon, P. Owen Ridge deep-water submarine landslides: Implications for tsunami hazard along the Oman coast. *Nat. Hazards Earth Syst. Sci.* **2013**, *13*, 417–424. [CrossRef]
41. Swapna, M.; Srivastava, K. Effect of Murray ridge on the tsunami propagation from Makran subduction zone. *Geophys. J. Int.* **2014**, *199*, 1430–1441. [CrossRef]
42. Lander, J.; Lowells, W.; Lockridge, P. A brief history of tsunami in the Caribbean Sea. *Sci. Tsunami Hazards* **2002**, *20*, 57–94.
43. Snead, R.E. Recent morphological changes along the coast of West Pakistan. *Ann. Assoc. Am. Geogr.* **1967**, *57*, 550–565. [CrossRef]
44. Wiedicke, M.; Neben, S.; Spiess, V. Mud volcanoes at the front of the Makran accretionary complex, Pakistan. *Mar. Geol.* **2001**, *172*, 57–73. [CrossRef]
45. Page, W.D.; Alt, J.N.; Cluff, L.S.; Plafker, G. Evidence for the recurrence of large-magnitude earthquakes along the Makran coast of Iran and Pakistan. *Tectonophysics* **1979**, *52*, 533–547. [CrossRef]
46. Monserrat, S.; Vilibić, I.; Rabinovich, A.B. Meteotsunamis: Atmospherically induced destructive ocean waves in the tsunami frequency band. *Nat. Hazards Earth Syst. Sci.* **2006**, *6*, 1035–1051. [CrossRef]
47. Rabinovich, A.B. Twenty-Seven Years of Progress in the Science of Meteorological Tsunamis Following the 1992 Daytona Beach Event. *Pure Appl. Geophys.* **2020**, *177*, 1193–1230. [CrossRef]

48. Heidarzadeh, M.; Sepic, J.; Rabinovich, A.; Allahyar, M.; Soltanpour, A.; Tavakoli, F. Meteorological Tsunami of 19 March 2017 in the Persian Gulf: Observations and Analyses. *Pure Appl. Geophys.* **2020**, *177*, 1231–1259. [CrossRef]
49. Ambraseys, N.N.; Melville, C.P. *A History of Persian Earthquakes*; Cambridge Earth Science Series; Cambridge University Press: Cambridge, UK, 1982.
50. Kumar, A. Natural hazards of the Arabian Peninsula: Their causes and possible remediation. In *Earth System Processes and Disaster Management*; Sinha, R., Ravindra, R., Eds.; Springer: Berlin/Heidelberg, Germany, 2013; pp. 155–180. [CrossRef]
51. Fritz, H.M.; Blount, C.D.; Albusaidi, F.B.; Al-Harthy, A.H.M. Cyclone Gonu storm surge in Oman. *Estuarine Coast. Shelf Sci.* **2010**, *86*, 102 –106. [CrossRef]
52. Shi, L.; Olabarrieta, M.; Nolan, D.S.; Warner, J.C. Tropical cyclone rainbands can trigger meteotsunamis. *Nat. Commun.* **2020**, *11*, 678. [CrossRef]
53. Okal, E.; Fritz, H.; Raad, P.; Synolakis, C.; Alshijbi, Y.; Al-Saifi, M. Oman Field Survey after the December 2004 Indian Ocean Tsunami. *Earthq. Spectra* **2006**, *22*, 203–218. [CrossRef]
54. Aguirre-Ayerbe, I.; Martínez Sánchez, J.; Aniel-Quiroga, I.; González-Riancho, P.; Merino, M.; Al-Yahyai, S.; González, M.; Medina, R. From tsunami risk assessment to disaster risk reduction–the case of Oman. *Nat. Hazards Earth Syst. Sci.* **2018**, *18*, 2241–2260. [CrossRef]
55. Aniel-Quiroga, I.; Álvarez-Gómez, J.A.; González, M.; Martínez Sánchez, J.; Parro, L.M.; Aguirre-Ayerbe, I.; Fernández, F.; Medina, R.; Al-Yahyai, S. Tsunami Hazard assessment and Scenarios Database for the Tsunami Warning System for the coast of Oman. *Nat. Hazards Earth Syst. Sci. Discuss.* **2018**, *2018*, 1–30. [CrossRef]
56. Rashidi, A.; Shomali, Z.H.; Dutykh, D.; Keshavarz Farajkhah, N. Tsunami hazard assessment in the Makran subduction zone. *Nat. Hazards* **2020**, *100*, 861–875. [CrossRef]
57. Barkan, R.; ten Brink, U.S.; Lin, J. Far field tsunami simulations of the 1755 Lisbon earthquake: Implications for tsunami hazard to the U.S. East Coast and the Caribbean. *Mar. Geol.* **2009**, *264*, 109–122. [CrossRef]
58. Barkan, R.; ten Brink, U. Tsunami simulations of the 1867 Virgin Island earthquake: Constraints on epicenter location and fault parameters. *Bull. Seismol. Soc. Am.* **2010**, *100*, 995–1009. [CrossRef]
59. Wen, R.; Ren, Y.; Li, X.; Pan, R. Comparison of two great Chile tsunamis in 1960 and 2010 using numerical simulation. *Earthq. Sci.* **2011**, *24*, 475–483. [CrossRef]
60. Tappin, D.R.; Watts, P.; Grilli, S.T. The Papua New Guinea tsunami of 17 July 1998: Anatomy of a catastrophic event. *Nat. Hazards Earth Syst. Sci.* **2008**, *8*, 243–266. [CrossRef]
61. Geist, E.L.; Titov, V.V.; Arcas, D.; Pollitz, F.F.; Bilek, S.L. Implications of the 26 December 2004 Sumatra–Andaman Earthquake on Tsunami Forecast and Assessment Models for Great Subduction-Zone Earthquakes. *Bull. Seismol. Soc. Am.* **2007**, *97*, S249–S270. [CrossRef]
62. Poisson, B.; Garcin, M.; Pedreros, R. The 2004 December 26 Indian Ocean tsunami impact on Sri Lanka: cascade modelling from ocean to city scales. *Geophys. J. Int.* **2009**, *177*, 1080–1090. [CrossRef]
63. Sugawara, D.; Goto, K. Numerical modeling of the 2011 Tohoku-oki tsunami in the offshore and onshore of Sendai Plain, Japan. *Sediment. Geol.* **2012**, *282*, 110–123. [CrossRef]
64. Wei, S.; Graves, R.; Helmberger, D.; Avouac, J.P.; Jiang, J. Sources of shaking and flooding during the Tohoku-Oki earthquake: A mixture of rupture styles. *Earth Planet. Sci. Lett.* **2012**, *333–334*, 91–100. [CrossRef]
65. Heidarzadeh, M.; Murotani, S.; Satake, K.; Ishibe, T.; Gusman, A.R. Source model of the 16 September 2015 Illapel, Chile, Mw 8.4 earthquake based on teleseismic and tsunami data. *Geophys. Res. Lett.* **2016**, *43*, 643–650. [CrossRef]
66. Heidarzadeh, M.; Ishibe, T.; Harada, T. Constraining the Source of the Mw 8.1 Chiapas, Mexico Earthquake of 8 September 2017 Using Teleseismic and Tsunami Observations. *Pure Appl. Geophys.* **2018**, *175*, 1925–1938. [CrossRef]
67. De Risi, R.; Goda, K. Simulation-Based Probabilistic Tsunami Hazard Analysis: Empirical and Robust Hazard Predictions. *Pure Appl. Geophys.* **2017**, *174*, 3083–3106. [CrossRef]
68. Ruiz, J.A.; Fuentes, M.; Riquelme, S.; Campos, J.; Cisternas, A. Numerical simulation of tsunami runup in northern Chile based on non-uniform k^{-2} slip distributions. *Nat. Hazards* **2015**, *79*, 1177–1198. [CrossRef]
69. Gonzalez, F.I.; Geist, E.L.; Jaffe, B.; Kânoğlu, U.; Mofjeld, H.; Synolakis, C.E.; Titov, V.V.; Arcas, D.; Bellomo, D.; Carlton, D.; et al. Probabilistic tsunami hazard assessment at Seaside, Oregon, for near- and far-field seismic sources. *J. Geophys. Res. Ocean.* **2009**, *114*. [CrossRef]

70. Sørensen, M.B.; Spada, M.; Babeyko, A.; Wiemer, S.; Grünthal, G. Probabilistic tsunami hazard in the Mediterranean Sea. *J. Geophys. Res. Solid Earth* **2012**, *117*. [CrossRef]
71. Pararas-Carayannis, G. The potential for tsunami generation along the Makran Subduction Zone in the Northern Arabian Sea. Case study: The earthquake and tsunami of November 28, 1945. *Sci. Tsunami Hazards* **2006**, *24*, 358–384.
72. Heidarzadeh, M.; Pirooz, M.D.; Zaker, N.H.; Yalciner, A.C. Preliminary estimation of the tsunami hazards associated with the Makran subduction zone at the northwestern Indian Ocean. *Nat. Hazards* **2009**, *48*, 229–243. [CrossRef]
73. Jankaew, K.; Atwater, B.F.; Sawai, Y.; Choowong, M.; Charoentitirat, T.; Martin, M.E.; Prendergast, A. Medieval forewarning of the 2004 Indian Ocean tsunami in Thailand. *Nature* **2008**, *455*, 1228–1231. [CrossRef]
74. Fujino, S.; Naruse, H.; Matsumoto, D.; Jarupongsakul, T.; Sphawajruksakul, A.; Sakakura, N. Stratigraphic evidence for pre-2004 tsunamis in southwestern Thailand. *Mar. Geol.* **2009**, *262*, 25–28. [CrossRef]
75. Atwater, B.F. Evidence for Great Holocene Earthquakes Along the Outer Coast of Washington State. *Science* **1987**, *236*, 942–944. [CrossRef] [PubMed]
76. Campos, C.; Beck, C.; Crouzet, C.; Demory, F.; Van Welden, A.; Eris, K. Deciphering hemipelagites from homogenites through anisotropy of magnetic susceptibility. Paleoseismic implications (Sea of Marmara and Gulf of Corinth). *Sediment. Geol.* **2013**, *292*, 1–14. [CrossRef]
77. Aguilar, I.; Beck, C.; Audemard, F.; Develle, A.L.; Boussafir, M.; Campos, C.; Crouzet, C. Last millennium sedimentation in the Gulf of Cariaco (NE Venezuela): Evidence for morphological changes of gulf entrance and possible relations with large earthquakes. *C. R. Geosci.* **2016**, *348*, 70–79. [CrossRef]
78. Donato, S.; Reinhardt, E.; Boyce, J.; Pilarczyk, J.; Jupp, B. Particle-size distribution of inferred tsunami deposits in Sur Lagoon, Sultanate of Oman. *Mar. Geol.* **2009**, *257*, 54–64. [CrossRef]
79. Shah-hosseini, M.; Morhange, C.; Beni, A.N.; Marriner, N.; Lahijani, H.; Hamzeh, M.; Sabatier, F. Coastal boulders as evidence for high-energy waves on the Iranian coast of Makran. *Mar. Geol.* **2011**, *290*, 17–28. [CrossRef]
80. Hoffmann, G.; Reicherter, K.; Wiatr, T.; Grützner, C.; Rausch, T. Block and boulder accumulations along the coastline between Fins and Sur (Sultanate of Oman): Tsunamigenic remains? *Nat. Hazards* **2013**, *65*, 851–873. [CrossRef]
81. Paris, R.; Naylor, L.A.; Stephenson, W.J. Boulders as a signature of storms on rock coasts. *Mar. Geol.* **2011**, *283*, 1–11, doi:10.1016/j.margeo.2011.03.016. [CrossRef]
82. Roeber, V.; Bricker, J.D. Destructive tsunami-like wave generated by surf beat over a coral reef during Typhoon Haiyan. *Nat. Commun.* **2015**, *6*, 7854. [CrossRef]
83. May, S.M.; Engel, M.; Brill, D.; Cuadra, C.; Lagmay, A.M.F.; Santiago, J.; Suarez, J.K.; Reyes, M.; Brückner, H. Block and boulder transport in Eastern Samar (Philippines) during Supertyphoon Haiyan. *Earth Surf. Dyn.* **2015**, *3*, 543–558. [CrossRef]
84. Kennedy, A.B.; Mori, N.; Yasuda, T.; Shimozono, T.; Tomiczek, T.; Donahue, A.; Shimura, T.; Imai, Y. Extreme block and boulder transport along a cliffed coastline (Calicoan Island, Philippines) during Super Typhoon Haiyan. *Mar. Geol.* **2017**, *383*, 65–77. [CrossRef]
85. Soria, J.L.A.; Switzer, A.D.; Pilarczyk, J.E.; Tang, H.; Weiss, R.; Siringan, F.; Manglicmot, M.; Gallentes, A.; Lau, A.A.; Cheong, A.Y.L.; et al. Surf beat-induced overwash during Typhoon Haiyan deposited two distinct sediment assemblages on the carbonate coast of Hernani, Samar, central Philippines. *Mar. Geol.* **2018**, *396*, 215–230. [CrossRef]
86. Cox, R.; Jahn, K.L.; Watkins, O.G.; Cox, P. Extraordinary boulder transport by storm waves (west of Ireland, winter 2013–2014), and criteria for analysing coastal boulder deposits. *Earth-Sci. Rev.* **2018**, *177*, 623–636. [CrossRef]
87. Atwater, B.F.; ten Brink, U.S.; Cescon, A.L.; Feuillet, N.; Fuentes, Z.; Halley, R.B.; Nuñez, C.; Reinhardt, E.G.; Roger, J.H.; Sawai, Y.; et al. Extreme waves in the British Virgin Islands during the last centuries before 1500 CE. *Geosphere* **2017**, *13*, 301–368. [CrossRef]
88. Hoffmann, G.; Grützner, C.; Schneider, B.; Preusser, F.; Reicherter, K. Large Holocene tsunamis in the northern Arabian Sea. *Mar. Geol.* **2020**, *419*, 106068. [CrossRef]
89. Hoffmann, G.; Rupprechter, M.; Balushi, N.A.; Grützner, C.; Reicherter, K. The impact of the 1945 Makran tsunami along the coastlines of the Arabian Sea (Northern Indian Ocean)—A review. *Z. Geomorphol. Suppl. Issues* **2013**, *57*, 257–277. [CrossRef]

90. Heck, N.H. List of seismic sea waves. *Bull. Seismol. Soc. Am.* **1947**, *37*, 269–286.
91. Kakar, D.; Naeem, G.; Usman, A.; Mengal, A.; Naderi Beni, A.; Afarin, M.; Ghaffari, H.; Fritz, H.; Pahlevan, F.; Okal, E.; et al. *Remembering the 1945 Makran Tsunami; Interviews with Survivors Beside the Arabian Sea*; United Nations Educational, Scientific and Cultural Organization (UNESCO): Paris, France, 2015; p. 79.
92. Adams, L.M.; Atwater, B.F.; Hasan, H. Karachi tides during the 1945 Makran tsunami. *Geosci. Lett.* **2018**, *5*, 25. [CrossRef]
93. Hasan, H.; Atwater, B.F.; Ahmed, S. A digital elevation model for simulating the 1945 Makran tsunami in Karachi Harbour. *Geosci. Lett.* **2018**, *5*, 23. [CrossRef]
94. Arjun, S.; Kalarani, D.P.; Praveen, S.S.; Reshmi, A.K.; Kurian, N.P.; Murthy, M.R.; Hameed, T.S.; Prakash, T.N. Numerical Simulation of the 1945 Makran Tsunami on the Southwest Coast and Lakshadweep Islands of India. *Mar. Geod.* **2011**, *34*, 68–76. [CrossRef]
95. Pendse, C.G. The Makran earthquake of the 28th November 1945. *India Meteorol. Dep. Sci. Notes* **1946**, *10*, 141–145.
96. Patel, V.M.; Dholakia, M.B.; Singh, A.P. Emergency preparedness in the case of Makran tsunami: A case study on tsunami risk visualization for the western parts of Gujarat, India. *Geomat. Nat. Hazards Risk* **2016**, *7*, 826–842. [CrossRef]
97. Rastgoftar, E.; Soltanpour, M. Study and numerical modeling of 1945 Makran tsunami due to a probable submarine landslide. *Nat. Hazards* **2016**, *83*, 929–945. [CrossRef]
98. Sarker, M.A. Numerical modelling of tsunami in the Makran Subduction Zone—A case study on the 1945 event. *J. Oper. Oceanogr.* **2019**, *12*, S212–S229. [CrossRef]
99. Okal, E.A.; Synolakis, C.E. Far-field tsunami hazard from mega-thrust earthquakes in the Indian Ocean. *Geophys. J. Int.* **2008**, *172*, 995–1015. [CrossRef]
100. Heidarzadeh, M.; Pirooz, M.D.; Zaker, N.H.; Synolakis, C.E. Evaluating tsunami hazard in the Northwestern Indian Ocean. *Pure Appl. Geophys.* **2008**, *165*, 2045–2058. [CrossRef]
101. Payande, A.R.; Niksokhan, M.H.; Naserian, H. Tsunami hazard assessment of Chabahar bay related to megathrust seismogenic potential of the Makran subduction zone. *Nat. Hazards* **2015**, *76*, 161–176. [CrossRef]
102. Browning, J.; Thomas, N. An assessment of the tsunami risk in Muscat and Salalah, Oman, based on estimations of probable maximum loss. *Int. J. Disaster Risk Reduct.* **2016**, *16*, 75–87. [CrossRef]
103. Schneider, B.; Hoffmann, G.; Reicherter, K. Scenario-based tsunami risk assessment using a static flooding approach and high-resolution digital elevation data: An example from Muscat in Oman. *Glob. Planet. Chang.* **2016**, *139*, 183–194. [CrossRef]
104. Suppasri, A.; Latcharote, P.; Al-Salem, K.; Pokavanich, T.; Jayaramu, Y.; Al-Enezi, A.; Toda, S.; Imamura, F. Tsunami Hazard Assessment for the Arabian Gulf from Earthquakes and Surface Landslides. *J. Jpn. Soc. Civ. Eng. Ser. B2 Coast. Eng.* **2016**, *72*, 1675–1680. [CrossRef]
105. El-Hussain, I.; Omira, R.; Al-Habsi, Z.; Baptista, M.A.; Deif, A.; Mohamed, A.M.E. Probabilistic and deterministic estimates of near-field tsunami hazards in northeast Oman. *Geosci. Lett.* **2018**, *5*, 30. [CrossRef]
106. Latcharote, P.; Al-Salem, K.; Suppasri, A.; Pokavanich, T.; Toda, S.; Jayaramu, Y.; Al-Enezi, A.; Al-Ragum, A.; Imamura, F. Tsunami hazard evaluation for Kuwait and Arabian Gulf due to Makran Subduction Zone and Subaerial landslides. *Nat. Hazards* **2018**, *93*, 127–152. [CrossRef]
107. Dutykh, D.; Mitsotakis, D.; Chubarov, L.B.; Shokin, Y.I. On the contribution of the horizontal sea-bed displacements into the tsunami generation process. *Ocean Model.* **2012**, *56*, 43–56. [CrossRef]
108. Rashidi, A.; Shomali, Z.H.; Keshavarz Farajkhah, N. Simulation of tsunami generation, propagation and run-up in the western Makran, Part 2: Simulation of the propagation and run-up. *J. Earth Space Phys.* **2018**, *44*, 509–521. [CrossRef]
109. Cisternas, M.; Atwater, B.F.; Torrejón, F.; Sawai, Y.; Machuca, G.; Lagos, M.; Eipert, A.; Youlton, C.; Salgado, I.; Kamataki, T.; et al. Predecessors of the giant 1960 Chile earthquake. *Nature* **2005**, *437*, 404–407. [CrossRef] [PubMed]
110. Carver, G.; Plafker, G. Paleoseismicity and Neotectonics of the Aleutian Subduction Zone—An Overview. In *Active Tectonics and Seismic Potential of Alaska*; American Geophysical Union (AGU): Washington, DC, USA, 2013; pp. 43–63. [CrossRef]
111. Kemp, A.C.; Cahill, N.; Engelhart, S.E.; Hawkes, A.D.; Wang, K. Revising Estimates of Spatially Variable Subsidence during the A.D. 1700 Cascadia Earthquake Using a Bayesian Foraminiferal Transfer Function. *Bull. Seismol. Soc. Am.* **2018**, *108*, 654–673. [CrossRef]

112. Burbidge, D.R.; Cummins, P.R.; Latief, H.; Mleczko, R.; Mokhtari, M.; Natawidjaja, D.; Rajendran, C.P.; Thomas, C. A Probabilistic Tsunami Hazard Assessment of the Indian Ocean Nations. *Geosci. Aust. Prof. Opin.* **2009**. Available online: http://pid.geoscience.gov.au/dataset/ga/68717 (accessed on 14 April 2020).
113. Heidarzadeh, M.; Kijko, A. A probabilistic tsunami hazard assessment for the Makran subduction zone at the northwestern Indian Ocean. *Nat. Hazards* **2011**, *56*, 577–593. [CrossRef]
114. Kijko, A.; Sellevoll, M.A. Estimation of earthquake hazard parameters from incomplete data files. Part II. Incorporation of magnitude heterogeneity. *Bull. Seismol. Soc. Am.* **1992**, *82*, 120–134.
115. El-Hussain, I.; Omira, R.; Deif, A.; Al-Habsi, Z.; Al-Rawas, G.; Mohamad, A.; Al-Jabri, K.; Baptista, M.A. Probabilistic tsunami hazard assessment along Oman coast from submarine earthquakes in the Makran subduction zone. *Arab. J. Geosci.* **2016**, *9*, 668. [CrossRef]
116. Hoechner, A.; Babeyko, A.Y.; Zamora, N. Probabilistic tsunami hazard assessment for the Makran region with focus on maximum magnitude assumption. *Nat. Hazards Earth Syst. Sci.* **2016**, *16*, 1339–1350. [CrossRef]
117. Rashidi, A.; Keshavarz Farajkhah, N. Probabilistic tsunami hazard assessment along the southeastern Iran coast. *Iran. J. Geophys.* **2019**, *13*, 1–13.
118. Gutscher, M.A.; Westbrook, G.K. Great earthquakes in slow-subduction, low-taper margins. In *Subduction Zone Geodynamics*; Lallemand, S., Funiciello, F., Eds.; Springer: Berlin/Heidelberg, Germany, 2009; pp. 119–133. [CrossRef]
119. Stein, S.; Okal, E.A. Ultralong Period Seismic Study of the December 2004 Indian Ocean Earthquake and Implications for Regional Tectonics and the Subduction Process. *Bull. Seismol. Soc. Am.* **2007**, *97*, S279–S295. [CrossRef]
120. McCaffrey, R. Global frequency of magnitude 9 earthquakes. *Geology* **2008**, *36*, 263–266. [CrossRef]
121. Cloos, M.; Shreve, R.L. Shear-zone thickness and the seismicity of Chilean- and Marianas-type subduction zones. *Geology* **1996**, *24*, 107–110. [CrossRef]
122. Ide, S. The proportionality between relative plate velocity and seismicity in subduction zones. *Nat. Geosci.* **2013**, *6*, 780–784. [CrossRef]
123. Zarifi, Z. Unusual Subduction Zones: Case Studies in Colombia and Iran. Ph.D. Thesis, University of Bergen, Bergen, Norway, 2006.
124. Løvholt, F.; Setiadi, N.J.; Birkmann, J.; Harbitz, C.B.; Bach, C.; Fernando, N.; Kaiser, G.; Nadim, F. Tsunami risk reduction—Are we better prepared today than in 2004? *Int. J. Disaster Risk Reduct.* **2014**, *10*, 127–142. [CrossRef]
125. Sawai, Y.; Namegaya, Y.; Okamura, Y.; Satake, K.; Shishikura, M. Challenges of anticipating the 2011 Tohoku earthquake and tsunami using coastal geology. *Geophys. Res. Lett.* **2012**, *39*. [CrossRef]
126. Sugawara, D.; Goto, K.; Imamura, F.; Matsumoto, H.; Minoura, K. Assessing the magnitude of the 869 Jogan tsunami using sedimentary deposits: Prediction and consequence of the 2011 Tohoku-oki tsunami. *Sediment. Geol.* **2012**, *282*, 14–26. [CrossRef]
127. Prendergast, A.L.; Cupper, M.; Jankaew, K.; Sawai, Y. Indian Ocean tsunami recurrence from optical dating of tsunami sand sheets in Thailand. *Mar. Geol.* **2012**, *295–298*, 20–27. [CrossRef]
128. Rajendran, C.P.; Rajendran, K.; Andrade, V.; Srinivasalu, S. Ages and relative sizes of pre-2004 tsunamis in the Bay of Bengal inferred from geologic evidence in the Andaman and Nicobar Islands. *J. Geophys. Res. Solid Earth* **2013**, *118*, 1345–1362. [CrossRef]
129. Malik, J.N.; Banerjee, C.; Khan, A.; Johnson, F.C.; Shishikura, M.; Satake, K.; Singhvi, A.K. Stratigraphic evidence for earthquakes and tsunamis on the west coast of South Andaman Island, India during the past 1000 years. *Tectonophysics* **2015**, *661*, 49–65. [CrossRef]
130. Maselli, V.; Oppo, D.; Moore, A.L.; Gusman, A.R.; Mtelela, C.; Iacopini, D.; Taviani, M.; Mjema, E.; Mulaya, E.; Che, M.; et al. A 1000-yr-old tsunami in the Indian Ocean points to greater risk for East Africa. *Geology* **2020**, *48*, 808–813. [CrossRef]
131. Schneider, B.; Hoffmann, G.; Falkenroth, M.; Grade, J. Tsunami and storm sediments in Oman: Characterizing extreme wave deposits using terrestrial laser scanning. *J. Coast. Conserv.* **2019**, *23*, 801–815. [CrossRef]
132. Nanayama, F.; Satake, K.; Furukawa, R.; Shimokawa, K.; Atwater, B.F.; Shigeno, K.; Yamaki, S. Unusually large earthquakes inferred from tsunami deposits along the Kuril trench. *Nature* **2003**, *424*, 660–663. [CrossRef] [PubMed]

133. Sawai, Y.; Satake, K.; Kamataki, T.; Nasu, H.; Shishikura, M.; Atwater, B.F.; Horton, B.P.; Kelsey, H.M.; Nagumo, T.; Yamaguchi, M. Transient Uplift After a 17th-Century Earthquake Along the Kuril Subduction Zone. *Science* **2004**, *306*, 1918–1920. [CrossRef] [PubMed]
134. Sawai, Y.; Kamataki, T.; Shishikura, M.; Nasu, H.; Okamura, Y.; Satake, K.; Thomson, K.H.; Matsumoto, D.; Fujii, Y.; Komatsubara, J.; et al. Aperiodic recurrence of geologically recorded tsunamis during the past 5500 years in eastern Hokkaido, Japan. *J. Geophys. Res. Solid Earth* **2009**, *114*. [CrossRef]
135. Carvajal, M.; Cisternas, M.; Catalán, P.A. Source of the 1730 Chilean earthquake from historical records: Implications for the future tsunami hazard on the coast of Metropolitan Chile. *J. Geophys. Res. Solid Earth* **2017**, *122*, 3648–3660. [CrossRef]
136. Zamora, N.; Gubler, A.; Orellana, V.; León, J.; Urrutia, A.; Carvajal, M.; Cisternas, M.; Catalán, P.; Winckler, P.; Cienfuegos, R.; et al. The 1730 Great Metropolitan Chile Earthquake and Tsunami Commemoration: Joint Efforts to Increase the Country's Awareness. *Geosciences* **2020**, *10*. [CrossRef]
137. Doxsey-Whitfield, E.; MacManus, K.; Adamo, S.B.; Pistolesi, L.; Squires, J.; Borkovska, O.; Baptista, S.R. Taking Advantage of the Improved Availability of Census Data: A First Look at the Gridded Population of the World, Version 4. *Pap. Appl. Geogr.* **2015**, *1*, 226–234. [CrossRef]
138. CIESIN. *Gridded Population of the World, Version 4 (GPWv4): Population Density Adjusted to Match 2015 Revision UN WPP Country Totals, Revision 11*; CIESIN: Palisades, NY, USA, 2018. [CrossRef]
139. Grezio, A.; Babeyko, A.; Baptista, M.A.; Behrens, J.; Costa, A.; Davies, G.; Geist, E.L.; Glimsdal, S.; González, F.I.; Griffin, J.; et al. Probabilistic Tsunami Hazard Analysis: Multiple Sources and Global Applications. *Rev. Geophys.* **2017**, *55*, 1158–1198. [CrossRef]
140. Gomberg, J.S.; Ludwig, K.A.; Bekins, B.; Brocher, T.M.; Brock, J.C.; Brothers, D.; Chaytor, J.D.; Frankel, A.; Geist, E.L.; Haney, M.M.; et al. *Reducing Risk Where Tectonic Plates Collide—U.S. Geological Survey Subduction Zone Science Plan*; US Geological Survey: Reston, VA, USA, 2017. [CrossRef]
141. Schluter, H.; Prexl, A.; Gaedicke, C.; Roeser, H.; Reichert, C.; Meyer, H.; von Daniels, C. The Makran accretionary wedge: Sediment thicknesses and ages and the origin of mud volcanoes. *Mar. Geol.* **2002**, *185*, 219–232. [CrossRef]
142. Burg, J.P. Geology of the onshore Makran accretionary wedge: Synthesis and tectonic interpretation. *Earth-Sci. Rev.* **2018**, *185*, 1210–1231. [CrossRef]
143. Hayes, G.P.; Moore, G.L.; Portner, D.E.; Hearne, M.; Flamme, H.; Furtney, M.; Smoczyk, G.M. Slab2, a comprehensive subduction zone geometry model. *Science* **2018**, *362*, 58–61. [CrossRef] [PubMed]
144. Wessel, P.; Smith, W.H.F. Free software helps map and display data. *Eos Trans. Am. Geophys. Union* **1991**, *72*, 441–446. [CrossRef]